The authors would like to thank the reviewers for their constructive comments. Please find our responses below.

Reviewer #1

This is a very interesting and important manuscript that describes an intercomparison of aerosol light absorption coefficient measurements taken with three miniature instruments for UAS deployment and two "reference" ground-based instruments. While I think that this manuscript describes very high quality and important work, the same cannot be said about the writing style, which could greatly benefit from extensive editing.

Following the advice of the reviewer, the manuscript has been re-edited and several typos were corrected. The structure of the manuscript has been altered as suggested with the "Instrumentation" section moved forward for clarity. Several sentences that were deemed confusing were omitted or changed, especially those speculating on the potential of UAS capabilities.

Lines 85-87: "In fact, the reduced size, weight, and power needs of these systems, along with the reduced cost of the platforms and instrumentation, make them suitable for these operations with huge potentials currently poorly demonstrated." This statement would benefit from some references.

This sentence was confusing and has been removed. Additionally, the referenced literature related to UAS-based absorption has been expanded.

Lines 87-94: Comments on "endurance and not risking the lives of crew" should be added.

This sentence has been removed from the revised manuscript.

Lines 94-96: "They have also the potential (yet not demonstrated) of the ground-based monitoring networks capabilities in providing long-term atmospheric observations." This is unclear to me, please reword.

Once more, this sentence seems to have caused confusion and has been omitted.

Lines 97-100: How was the "vertical distribution of aerosol absorption" performed???

This is now clarified in the revised manuscript. This sentence now reads "we focus on vertical distributions of aerosol absorption, measured with miniature absorption sensors onboard small and medium-size UAS during two intensive field campaigns at contrasting locations in the Eastern Mediterranean". This can be found in lines 112-116 of the revised manuscript.

Lines 347 & 359: "Angstrom" or "angstrom"? How about "Ångström"?

This word has been replaced, as suggested by the reviewer, in the revised manuscript

Line 515: "agreement" or should this read "correlation"?

In the first version of the manuscript, the term "agreement" was confusing and has been replaced by the term "correlation" throughout as suggested.

Reviewer #2

The manuscript fits within the scope of Atmospheric Measurement Techniques and the insights are novel enough to justify publication. There are though a number of details that should be addressed before the publication and the manuscript should be thoroughly checked.

The authors use an atypical structure (sections) for AMT, or any journal for that matter. This is fine but it would be critical to detail in the text when something gets explained in a later section. e.g. The field campaigns should somehow mention that the UAS will discussed later as one expect to read details when something like multi-copter comes up. Alternatively may be the authors should consider to first discuss the tools, then the platforms before discussing the field campaigns as the primary focus here should be on tools, platforms and measurements not on the field campaigns.

The authors agree that the form of the manuscript did not assist the reader. In the revised manuscript the "Instrumentation" section now precedes that of the "Campaigns".

The current state of the art and background are extremely poorly described in the introduction. The paper is very misleading on how novel BC measurements by UAV are. It gives an impression that this is very novel when in reality BC has been measured on UAVs for more than 10 years (see Corrigan et al., 2008). This is just not proper. You mention Bates for the STAB but fail to mention that the Bates paper is not only this instrument but this instrument on a UAV. Your paper has to acknowledge what is out there, what instruments flew on what platforms etc.. Also in regards to the discussion of the vertical profile observations, there are studies to compare to, both UAV and balloon (besides Bates, Corrigan, there Po Valley Ferrero et al., 2014).

The above statement is a misunderstanding. The authors consider novel the use of miniature sensors onboard small size UAS. Small UAS are considered those with a gross weight smaller than 25 kg as suggested by the FAA. In the revised manuscript, there is a clearer description of this notion so to avoid confusion. The term "small UAS" is used and in Section 2.1 this is clarified. Furthermore, there is a distinction between standard (rack) size and small sensors (Lines 82-88 of the revised manuscript).

Taking into account the above comment, we have substantially edited the relevant paragraph in the introduction (see revised manuscript) and included several publications concerning absorption vertical profiles, either using UAS or tethered balloons. (Lines 82-96).

It should be noted that the main focus of this work is to present the instrument intercomparison. A comparison between the findings from the campaigns described in this work and those already found in the literature is beyond the scope of this study. Our intention is to focus on the results of both campaigns in a future separate publication.

Some statements are misleading and/or too qualitative in the discussion. The authors confuse correlation with agreement (Line 513 discussion figure 4), MAAP and AE33 are not in agreement if there is a 20% bias. The measurements are well correlated but the values are substantially off, systematically yes but still the values are not in agreement at all. Also, the authors use too many qualitative statements like "excellent" when it is unclear what excellent means. Things are statistically significant or not.

The reviewer is correct. The term "agreement" has been replaced by the term "correlation" throughout the manuscript. Additionally, a Welch's t-test, used in cases when populations of unequal variances are to be compared, was employed to deduct the significance of the differences discussed in this work.

Finally, one has to hope that the authors were more careful in their experiments than in the preparation of the manuscript. The manuscript needs a serious re-read with attention to detail for text formatting, typos, format of references and completeness of references cited. A few items are in details but the list is not certainly exhaustive.

Hewewith, we would like to mention that the high-quality of the data presented in our work has been assured in several ways (reference instruments, sample conditioning (dryer), airborne and inflight intercomparison). The authors acknowledge indeed that several small errors were present in the old manuscript, which has undergone extensive re-editing. This includes, among others; correction of typos, confusing sentences to be rephrased or omitted, uniform spacing and text formatting throughout.

L29-31 "the measured signal of the three sensors was converted into absorption coefficient,... and, when applicable, to signal saturation corrections following the suggestions of the manufacturers." Please reformulate, the signal was not converted to corrections but you applied corrections.

This sentence has been edited and in the revised manuscript and now reads at Line 31:" The measured signal of the miniaturized sensors was converted into the absorption coefficient and equivalent black carbon concentration (*eBC*). When applicable, signal saturation corrections were applied, following the suggestions of the manufacturers."

L58 redefine abbreviations at first use in the main text (here BC)

BC is now defined in Line 56. The manuscript was checked to ensure that each abbreviation was defined at first use. The authors include a nomenclature table to assist the reader with the abbreviations employed in the text.

L64-69 This is a poor representation of the existing methods and partly misleading ... The sunset is thermal AND optical and there are thermal optical transmission and thermal optical reflection... see AMT papers on the subjects. For just evolved gas phase there are the old commercial systems such as the R&P analyzer, there is the DRI analyzer. You only give 2 Sunset papers. This is not critical but just weird and actually wrong.

This sentence was reformulated by removing the reference of the two Sunset papers, mentioning briefly the thermal-optical techniques, which are now replaced bya reference to Lack et al., 2014, a review paper that describes in-depth the techniques for measuring the concentration of black carbon.

L68 Please check also all your references throughout the manuscript. Here the Petzold and Moosmueller refs are both missing in the literature cited.

We thank the reviewer for identifying this omission. The revised manuscript was thoroughly checked. All references were additionally checked for abiding with the AMT format.

L123 Athens campaign. If you keep the structure with first field campaigns then instruments then please reference at the mention of multicopter that you will provide details later, idem later on for the Cyprus study UAS.

This structure has changed in the revised manuscript, with the instrumentation section preceding that of the campaign.

L128 The 2kg payload limitation is confusing as the Table says different. Please elaborate and please elaborate and clarify which instrument this refers to.

The reviewer is correct as these two statements correspond to different payloads. Line 407 in the revised manuscript (used to be Line 128) refers to the instrument only assuming an extra 2 kg for batteries, the dryer, and the inlet. In Table 1 the net payload was specified. The authors acknowledge that this sentence was confusing and have rephrased it to "Due to payload restrictions (2 kg maximum for scientific instrumentation and another 2 kg payload for the batteries, dryer and inlet),…".

L371 section on miniature monitor descriptions. Please discuss them all 3 Currently hardly any description is here on the DWP and please be consistent by providing/discussing weight of all 3 of them. Essentially give the same information and same level of detail for all 3 consistently. This would be most useful.

As proposed, information on DWP has been added. In specific, the following sentences are now found in Lines 329-333 of the revised manuscript "The DWP has been constructed as a modification of the AE51, by placing an additional light source, emitting at 370 nm. Additionally, the sampling flow rate has been increased to 2 L min^{-1}, by replacing the original AE51 pump, with an external whose flow rate is controlled by a critical orifice. The external pump resulted in additional weight to DWP. "

The UAS platforms in Table 1 should include manufacturer.

This information has been included in the revised manuscript

Table 1: typo km not k, formatting: align text to center of pictures

The typo has been corrected

Table 1. define abbreviations at first use

These have been defined and have been included in the nomenclature table.

Figure 1: provide the source of the maps and pictures and ensure you have the rights

Figure 1 (formerly Fig. 2) is owned by the authors. Figure 2 (formerly Fig. 1) is owned by Google which encourages the use of its maps for scientific publication. Google policy can be summarized as follows "Due to limited resources and high demand, we're

unable to sign any letter or contract specifying that your project or use has our explicit permission. As long as you follow the guidance on this page, and attribute the content correctly, feel free to move forward with your project." Which can be found at https://www.google.com/permissions/geoguidelines/

Figures 4,5,6,7: could you provide error bars on the values. If they are smaller than the symbols used then please state so in the legend.

Error bars have been added in Fig. 4,5,6,7 corresponding to one standard error from the mean. It is noted that if one standard deviation from the mean was plotted then Fig 5, 6, and 7 would become unreadable; mainly because AE51 is quite noisy. Therefore, to keep a uniform and concise format throughout, all figures exhibit one standard error from the average, while standard deviation is reported in the text. Under this configuration, the symbols concerning STAP and DWP in Fig. 5 and 6 are larger than the error bars, which is denoted in the legend of each figure.

List of changes applied in the revised manuscript

The original manuscript has undergone extensive editing, as can be seen in the tracked changes version found below.

Major changes include:

- **Text**

Several references were added in the revised manuscript concerning vertical absorption profiles using UAS or balloons (Line 90-96), manned aircrafts (Line 79-81), mathematical tests applied to examine the statistical significance of the reported differences (Line 545=550) and a recent publication on the discrepancies of RH on absorption measurements (Line 538).

The section "Instrumentation" precedes that of "Sampling sites".

Abbreviated physical properties such as *eBC*, b_{abs} are now all in Italic.

Line 448-455. A paragraph referring to LIDAR measurements has been moved from the "Ground based reference instruments" to the "Cyprus Campaign"

Line 329-339: The discussion regarding DWP has been expanded.

Lines 563-569: An explanation is provided as to why small differences in eBC measurements from AE33 and MAAP grow large with respect to the absorption coefficient. In addition the revised manuscript the values used to derive the absorption coefficient are now mentioned (see eg Line 700-701)

Lines 839-845: One of the basic findings of this work is now further analyzed in the "Conclusions"

- **Figures**

Figure 1 in the original manuscript is listed in the revise manuscript as Fig. 2

Figure 2 in the original manuscript is listed in the revise manuscript as Fig. 1

Figure 2 denotes source of the images

Figures 4, 5, 6 and 7 include error bars. The caption of each figure is also updated

Fig. 4 includes information on the slope of the comparison

Fig 9 lower panel now shows attenuated backscatter instead of arbitrary signal

A new figure showing the comparison of MAAP against AE33 at 637 nm is included in the supplement. It has been listed as Suppl. Fig. 2. In the revised manuscript Suppl. Fig 2 is now listed as Suppl. Fig. 3, Suppl. Fig 3 is now listed as Suppl. Fig. 4, etc.

- **Tables**

Table 1 includes information on the manufacturer as suggested by Reviewer #2.

Table 1 caption includes information on UAS size.

MTOW is now defined as a footnote of Table 1.

In the revised manuscript, Table 2 first column is “Instrument name” and the second “Manufacturer”

A footnote has been added in Table 3 to note that Weight refers to the weight of the instrument alone.

On-flight intercomparison of three miniature aerosol absorption sensors using Unmanned Aerial Systems (UAS)

Michael Pikridas[1], Spiros Bezantakos[1], Griša Močnik[2, 3], Christos Keleshis[1], Fred Brechtel[4], Iasonas Stavroulas[1,5], Gregoris Demetriades[1], Panayiota Antoniou[1], Panagiotis Vouterakos[1], Marios Argyrides[1], Eleni Liakakou[5], Luka Drinovec[2,3], Eleni Marinou[6,7], Vassilis Amiridis[6], Mihalis Vrekoussis[1,8,9], Nikolaos Mihalopoulos[1,5] and Jean Sciare[1]

[1]*Energy Environment and Water Research Center, The Cyprus Institute, Nicosia 1645, Cyprus*

[2]*Aerosol d.o.o., 1000 Ljubljana, Slovenia*

[3]*Jozef Stefan Institute, 1000 Ljubljana, Slovenia*

[4]*Brechtel Manufacturing Inc., 1789 Addison Way, Hayward, CA 94544 U.S.A.*

[5]*Institute for Environmental Research and Sustainable Development, National Observatory of Athens, 15236, Athens, Greece*

[6]*Institute for Astronomy, Astrophysics, Space Applications and Remote Sensing (IAASARS), National Observatory of Athens (NOA), Athens, Greece*

[7]*Institute of Atmospheric Physics, German Aerospace Center (DLR), 82234 Weßling, Oberpfaffenhofen, Germany*

[8]*Institute of Environmental Physics, University of Bremen, Otto-Hahn-Allee 1, D-28359 Bremen, Germany*

[9]*Center of Marine Environmental Sciences - MARUM, D-28359 Bremen, Germany*

The present study investigates and comparesfor the first time, the ground and in-flight performanceperformances of three miniaturized aerosol absorption sensors integrated on-board of small size Unmanned Aerial Systems (UAS). These sensors were evaluated during two contrasted field campaigns performed respectively at an urban site, (Athens, Greece) impacted mainly by local traffic and domestic wood burning sources (Athens, Greece), and at a remote regional background site, (Agia Marina, Cyprus) impacted by long-range transported sources including dust (Cyprus Atmospheric Observatory, Agia Marina Xyliatou, Cyprus).

The miniaturizedthree sensors were first intercompared at the ground -level against two commercially available instruments (MAAP and AE33) used as a reference. The measured signal of the miniaturizedthree sensors was converted into the absorption coefficient and, equivalent black carbon concentration (*eBC*). When) and, when applicable, to signal saturation corrections were applied, following the suggestions of the manufacturers. The aerosol absorption sensors exhibited similar behavior against the reference instruments during the two campaigns, despiteDespite the diversity of the aerosol origin, chemical composition, sources, and concentration levels. during the two campaigns, the aerosol absorption sensors exhibited similar behavior against the reference instruments. The deviation from the reference, during both campaigns, concerning (*eBC*) mass was less than 8% while for the absorption coefficient was at least 15%. This indicates%, suggesting that those miniature sensors that report black carbonBC mass are tuned/corrected to measure more accurately *eBC* rather than the absorption coefficient. which deviated at least 15%.

The overall potential use of miniature aerosol absorption sensorssensor on-board small UAS is also illustrated here. UAS-based absorption measurements were used to investigate the vertical distribution of *eBC* over Athens up to 1 km above sea level during January 2016, exceedingreaching the top of the planetary boundary layer (PBL). Our results revealhighlighted a heterogeneous boundary layer concentration of absorbing aerosol within the PBL intensified especially in the early morning hours due towith the concurrent peak traffic emissions at ground-level and the fast development of the boundary layer. After the full development of the PBL, homogenous concentrations are observed from the 100m a.g.l. to the PBL top. Vertical homogeneity was achieved when the boundary layer depth became stable.

1. Introduction

Atmospheric aerosol particles scatter and absorb incoming solar radiation, thus directly affecting the radiative balance of the atmosphere (Haywood and Boucher, 2000). Their contribution to climate change is still associated with large uncertainties when estimating their radiative forcing (RF) (Bond et al., 2013; IPCC, 2013). A major contributor to these uncertainties is the RF induced by black carbon (BC), which exhibits a relative standard deviation exceeding 40% among different numerical climate models (Myhre et al., 2013). The BC direct RF has been estimated to be 0.71 Wm^{-2} with an uncertainty range of 0.08 to 1.27 Wm^{-2} (Bond et al., 2013), while in a more recent study it ranged from 0.14 to 1.19 Wm^{-2} (90% confidence interval) with an average value of 0.53 Wm^{-2} (Wang et al., 2016). Major factors responsible for the wide range of the BC's RF estimates include the inaccurately predicted BC emission rates, poorly understood interactions of BC with clouds, and the inaccuracy in representing its vertical distribution (Bond et al., 2013). In addition, BC has been identified to reduce the albedo of snow surfaces (Hadley and Kirchstetter, 2012) and to suppress the turbulence of the boundary layer (Wilcox et al., 2016).

An array of techniques and instruments are employed worldwide with the aim to increase the spatial and temporal resolution of BC observations. The instrumentation employed is based on different operating principles, including off-line or near-real-time methods for measuring Elemental Carbon (EC), such as thermal-optical reflectance/transmittance (cf. Lack et al., 2014 and references therein for more details) as well as on-line, real-time methods. The latter are mainly based on the aerosol light-absorbing properties of BC (cf. Moosmüller et al., 2009; Petzold et al., 2013; Lack et al., 2014 and references therein for more details).

Most of the aerosol absorption observations available in the literature are conducted at ground level. Consequently, they lack critical information regarding the vertical distribution of aerosol absorption a key parameter to constrain atmospheric models and accurately assess aerosol radiative forcing effects (Samset et al., 2018). One way to fill this gap is by conducting manned airborne aerial absorption measurements (Seinfeld et al., 2004; Subramanian et al., 2010; Freney et al., 2014; Kassianov et al., 2018; Katich et al., 2018; Sedlacek et al., 2018). However, these are costly and cover a limited period of observations. In the pioneering work of Corrigan et al. (2008), vertical absorption profiles over the Indian Ocean were measured using parts from a standard (rack) size instrument onboard a medium scale (25-150 kg) unmanned aerial system (UAS). Since

then, the size and weight of absorption monitors have been reduced, and the use of lightweight miniaturized sensors on-board of small UAS or tethered balloons provides cost-effective alternatives able to fill the measurement gap and to enhance the vertical and temporal density of aerosol absorption observations. A UAS is defined as small if its gross weight is less than 25 kg (US Federal Aviation Administration, CFR 14). Vertical aerosol absorption observations using small UAS or tethered balloons have been already conducted in different regions such as the Indian Ocean (Höpner et al., 2016), India (Bisht et al., 2016), the Arctic (Bates et al., 2013; Ferrero et al., 2016), Italy (Ferrero et al., 2011; 2014), Poland (Chilinski et al., 2016), and China (Ran et al., 2016). These measurements can be further used to obtain the vertically resolved heating rate, including contributions from different sources and carbonaceous aerosol fractions (Ferrero et al., 2014; 2018). The employment of UAS in some of the above-mentioned campaigns proves to be a viable option to obtain information on aerosol absorption vertical distribution. Even though small UAS are subject to significant payload restrictions, compared to manned aircrafts, they have a distinct advantage over their manned counterparts in terms of relatively low platform and operation cost, capability to perform autonomous flight operations, the ability to fly closer to the ground with greater spatial accuracy and to collect spatially dense data (due to low speed operation) under reduced workload (Villa et al., 2016). In addition, they have the advantage of better controllability in comparison to balloons and zeppelins, since the latter are more delicate at stronger winds (Inoue et al., 2000; Jensen et al., 2007). In terms of instrumentation, ground-based aerosol absorption instruments have been qualified in many intercomparison studies (e.g. Müller et al., 2011). On the contrary, their miniaturized counterparts' behavior is yet poorly demonstrated in-flight. The measurement quality delivered by these sensors during flight is challenged by fast changes in pressure, temperature, and humidity, which are difficult to assess from concurrent ground-level measurements.

In this work, we focus on vertical distributions of aerosol absorption, measured with miniature absorption sensors onboard small and medium-size UAS during two intensive field campaigns at contrasted locations in the Eastern Mediterranean; an urban site (Athens, Greece) and a remote regional background site (Cyprus Atmospheric Observatory, CAO, Cyprus). The vertical distribution of aerosols in the Eastern Mediterranean is of particular importance because it lies at the crossroads of diverse air masses (Lelieveld et al., 2002) carrying aerosol of different composition, including mineral dust from Africa and the Middle East, pollution from Europe and the nearby Middle East, and marine aerosol (Erel et al., 2006; Gerasopoulos et al., 2007; Kalivitis et al., 2007). In addition, aerosol absorption measurements, either ground or aerial-based, are rather scarce in the region. The sites were selected to represent two different and contrasted sources of ambient aerosol, with high concentration levels of freshly emitted BC from traffic and/or biomass burning (domestic heating) in Athens and low concentrations of aged regionally transported aerosol, occasionally mixed with moderate levels of dust in Cyprus.

Aerosol vertical profiles were monitored~~. Aerosol vertical profiles were performed~~ using several types of fixed and rotary wing UAS. In addition to the~~wings unmanned~~ aerial observations~~systems (UAS). In this work~~, three miniature attenuation monitors were also characterized against ground -based commercial instruments.

Secondly~~Instead of characterizing their performances under controlled conditions~~, these miniature sensors~~monitors~~ were compared~~tested~~ and characterized in~~intercompared on~~-flight with different UASs and diverse absorbing aerosol concentrations and types.

~~2. Sampling Sites~~

~~Sampling was conducted at two contrasted locations in the Eastern Mediterranean basin; an urban site (Athens, Greece) for a 1-week intensive period starting from 14 January 2016 and a background location in Cyprus for a 1-month intensive campaign in April 2016.~~

~~2.1 Athens campaign~~

~~In the framework of the European project ACTRIS 2 (Aerosols, Clouds, and Trace Gases Research Infrastructure), three miniaturized absorption instruments were tested and intercompared for a period of one week (14-21 January 2016) onboard UAS over Athens, a city highly impacted by strong UV-absorbing domestic heating biomass burning aerosols during winter (Florou et al., 2017; Fourtziou et al., 2017). Flights were conducted at Lofos Nymphon (37°58'19.68"N - 23°43'5.32"E) situated at the historical center of Athens, a metropolitan area of more than 4,000,000 inhabitants. Lofos Nymphon is a small rock plateau inside a small forested area (Fig. 1), at a 50 m elevation from its surroundings. Traffic roads, marked with red lines on Fig. 1, are located westerly of the site. The closest traffic road is 150 m away from the measuring site. In order to comply with air space restrictions made by the Hellenic civil aviation authorities at Lofos Nymphon, a multicopter, described in detail in Section 3.1.3, was selected for its capacity to take-off and land vertically.~~

~~A total of 26 flights were performed during periods without precipitation or strong winds, lasted for 15min each reaching as high as 1 km above sea level (a.s.l.) altitude limit set by the Hellenic civil aviation authorities.~~

~~During this campaign, the flight strategy has been elaborated as the following: Two early morning flights were performed at an interval of c.a. one hour starting at sunrise (05:00 UTC) to investigate the stratification of the atmosphere (boundary layer, low free troposphere). Two late-afternoon flights ending approximately at sunset (16:00 UTC) were performed to investigate the vertical mixing of urban emissions in the atmospheric column. On 19 January 2016, intensive (hourly) flights were performed to investigate the impact of the diurnal development of the boundary layer on the vertical distribution of absorbing aerosols. These flights are further discussed in Section 7.~~

~~Due to payload restrictions (2 kg maximum for scientific instrumentation), not all the miniature monitors could fly simultaneously. The monitors that could not fly were operated at the co-located National Observatory monitoring station at Lofos Nymphon, together with two commercially available instruments (Magee Scientific AE33 and Thermo MAAP). In addition, the absorption monitor on board the multi-copter has been measuring at ground level during 2-3 min before and after each flight for a direct comparison against ground-based instruments.~~

~~2.2 Cyprus campaign~~

In the framework of the European project BACCHUS (Impact of Biogenic versus Anthropogenic emissions on Clouds and Climate; towards a Holistic UnderStanding) a 1-month campaign (30 March – 28 April 2016) was performed at the Cyprus Atmospheric Observatory (CAO, 35° 2'17.97"N – 33° 3'28.50"E), a remote regional background site at the Agia Marina Xyliatou in Cyprus.

Vertical profiles of aerosol absorption were performed in a dedicated UAS airfield (35° 5'41.93"N – 33° 4'54.26"E) located at approximately 7 km north of the Cyprus Atmospheric Observatory (Fig. 1). The airfield, shown in Fig. 2, is associated with a 500 m radius (in x-y plane) UAS airspace and an additional 500 m radius buffer zone, yielding a total of 1 km radius flight zone granted by the Cypriot civil aviation authorities and extending up to a height of approximately 2.4 km a.g.l. (2.7 km a.s.l.).

The UAS flight strategy was designed at characterizing the boundary layer and free troposphere with respect to aerosol absorption, number size distribution, and ice nuclei (IN) concentrations. More information from the UAS-based IN measurements can be found in Schrod et al. (2017). UAS-based aerosol number size distribution are presented and discussed in Mamali et al. (2018). The typical UAS flight period usually spanned from sunrise (05:00 UTC) to 09:00 UTC. Two types of fixed wing UASs were used during this campaign; two skywalker UAS (Model X8) and one Cruiser UAS (see section 3.1). Skywalker X8 flights typically lasted 30 min, while each Cruiser flight lasted between 1-1.5 h. 2Vertical profiles were performed almost on a daily basis provided meteorological conditions were favorable, and engaged a team of eight persons (two pilots, two ground control station operators, two electronic/mechanical engineers and two scientific staff for the operation of the miniaturized instruments). In this work, only the absorption measurements will be examined corresponding to a total of 17 flights performed with Skywalker X8 and 6 flights with the Cruiser.

Ground based absorption measurements were conducted at CAO using two commercially available instruments (Magee Scientific AE33 and Thermo MAAP, see section 3.2.2). CAO is located 6.74 km southerly and at a 200 m elevation higher of the airfield (Fig. 1). Because of no significant local contamination sources in the surrounding area (Kleanthous et al., 2014; Pikridas et al., 2018), it has been assumed that atmospheric composition at CAO and the UAS airfield were similar, allowing a direct comparison between ground and airborne measurements. During this campaign, regional dust transport originating from Africa was identified on two occasions, during 9th and 20th of April 2016 respectively (Schrod et al., 2017).

3. Instrumentation

23.1 Unmanned Aerial System Types

ThreeAs mentioned above, three types of unmanned aerial systems (UAS) have been used in this study; they differ with respect to the payload, autonomy, wing type, and landing requirements. Their specifications and capabilities, described below, are summarized in Table 1. In addition and as mentioned before, UAS are characterized as small when their gross weight is less than 25 kg and medium if their gross weight ranges between 25 - 150 kg (US Federal Aviation Administration, CFR 14). Despite having the ability to reach altitudes higher than 2 km above ground level (a.g.l.),, the UASs were limited to 1 and 2 km during the Athens and CyprusCAO campaigns, respectively, due to restrictions posed by the civil aviation authorities.

23.1.1 UAS “Cruiser”

The Cruiser is a medium-size fixed-wing UAS (Table 1) with a payload capacity up to 12 kg which includes alsoboth the weight of the fuel to power the engine and the battery used for the instrumentation. The Cruiser’s payload bay, the available space inside the UAS, measures 1.3 m × ×0.23 m × ×0.34 m (LxWxH). The UAS features) and it comes with a wingspan of 3.8 m. It has been configured with an internal combustion two-stroke engine placed in a pushpusher configuration enabling an that can climb up to 3-4 km altitude ceiling of 4 km and with a maximum take-off weight of 35 kg. Depending on payload and environmental conditions the Cruiser can reach a flying endurance up to 8 hours. During the flight, atmospheric sampling occurs at a velocity of 28±5 m s^{-1} which is the typical cruising air-speed of this type of UAS. Under its current configuration the environmental conditions to ensure a safe operation are limited to winds up to 13 m s^{-1} and temperatures abovebelow the dew point in order to prevent icing on the engine’s carburetorcarburettor. However, the engine can be upgraded with an electronic fuel injection system in order to fly under icing conditions and thus to higher altitudes. The Cruiser is equipped with an autopilot system (Micropilot MP2128G2) which includes all the sensors and telecommunication systems (e.g. GPS, barometric altimeter, accelerometer, air-speed sensor, electronic compass, modems, antennas) that allows autonomous flights with real-time monitoring and control from the ground providing that predetermined flight plans are set. At any time, the UAS operator is able to modify the active flight plan in real-time. In addition, the system is capable of detecting faults and alter its flight plan accordingly (e.g. automatically return to home upon communication loss). The modular design of the Cruiser facilitates switching instruments between scientific missions provided that the total mass does not exceed the payload limit. To support its multi-instrument capability, a central data acquisition system built around the National Instruments controller, myRIO with a variety of interface possibilities and a Graphical User Interface (GUI) has been developed. The NI graphical programming language of Labview (from National Instruments) has been utilized to develop the GUI with capabilities of real-time visualization of the instrumentation data as well as controlling and automation of the on-board instruments. All the instruments and avionics sensitive to vibration shake have been mounted into the Cruiser fuselage using special anti-vibration dampers in order to insulate them fromisolate the high-frequency oscillations produced by the UAS engine. Vibration insulationisolation is essential in order to improve the flying reliability of the UAS as well as to keep the quality of the scientific measurements to its higher standards.

Due to the Cruiser’s size, a flat (ideally paved) runway is required for take-off and landing. During the Cyprus campaign, the Cruiser was taking-off and landing on Cyprus Institute's private runway (see Fig. 1the CyI’s private runway (see Fig. 2). Along with other aerosol instruments (Ice Nuclei sampler, Optical particle counter), the Cruiser UAS carried one miniature absorption instrument (AE51, see section 3.2.3).

23.1.2 UAS “Skywalker X8”

The Skywalker X8 is a small delta-wing type UAS with an electric motor providing the propulsion. Made fromby foam, it is a much smaller and lower cost UAS comparedcomparing to the Cruiser. Its wingspan is 2.10 m and its maximum take-off

weight is about 5.5 kg. It can fly for approximately one hour up to 3 km altitude with a payload of c.a. 3 kg, which includes the battery (14.8V Lithium Polymer, 9Ah) that powers the motor. This UAS is equipped with the same avionics as the Cruiser, maintaining all of its advanced automation characteristics. The Skywalker X8 can take-off using a bungee launcher catapult system and can land on its belly on any flat surface, thus minimizing the requirements for a specialized aerodrome. ~~. The skywalker X8 UAS has been operating exclusively during the Cyprus campaign and carried only one miniature absorption instrument (DWP, see section 3.2.3).~~

23.1.3 UAS "Multicopter S1000+"

A modified version of the commercially available octocopter DJi S1000+ was used during the Athens campaign to overcome strong constraints related to a limited ground area for~~to~~ take-off and landing, and flying in the limited air space. This platform has been optimized to reach an altitude up to 1 km above sea level (a.s.l.) ~~.~~ for a maximum take-off weight of 11 kg and a payload of 4 kg including the motor battery (22V Lithium Polymer, 22Ah). In order to ensure that sampling was not influenced by the turbulence created by the octocopter's blades, the sampling inlet was extended by 1 m out of the propeller downdraft~~flow~~. This distance ensured representative sampling while ascending.~~during ascend.~~ However, during descent, this length was not sufficient to avoid the created vortex when~~if~~ a columnar path was followed. During the Athens campaign, the landing site was near the edge of a cliff and inside an archaeological area where pedestrians could freely access (Fig. 2)~~,~~ prohibiting deviation from a columnar flight path. ~~(Fig. 1).~~ As a result, the quality of the descent flights was compromised at the expense of safety and thus only ascending flights are used in this work.

23.2 Aerosol absorption instrumentation

23.2.1 Principle of operation

~~Aerosol absorbing component can be apportioned in real-time using optical methods.~~ The most widely used instruments for the determination of the~~method, utilizes an~~ aerosol absorption coefficient are filter photometers. They sample ambient air through a filter,~~sample-laden filter area~~ where the sample is collected. The filter is illuminated and the light ~~is~~ transmitted through the filter is measured. Transmission of the sample-laden filter is normalized to the transmission of the sample-free filter~~. Additionally, light is simultaneously transmitted via an aerosol-free (unloaded) filter spot~~ (reference signal) and the attenuation is calculated based on Eq. 1.

$$ATN(\lambda) = 100 \times \ln\left(\frac{I_{ref}(\lambda)}{I_{sample}(\lambda)}\right) \qquad \textbf{Eq. 1}$$

where $I_{ref}(\lambda)$ and $I_{sample}(\lambda)$ are the reference and sample light intensities at the detectors under the filter~~signals~~, respectively, and $ATN(\lambda)$ the attenuation at wavelength λ. The attenuation rate dATN(λ)/dt (calculated from consecutive measurements) determines the attenuation coefficient ($b_{atn}(\lambda)$) based on Eq. 2.

$$b_{atn}(\lambda) = \frac{A}{100Q}\frac{dATN(\lambda)}{dt} \quad b_{atn}(\lambda) = \frac{A \cdot dATN(\lambda)}{100Q \cdot dt}$$

Eq. 2

where A is the sample spot area, Q the airflow rate and dt the time period for which the attenuation change is considered. It typically equals to 1s for all the miniaturized instruments examined in this study. The instrument specific $b_{atn}(\lambda)$ can be converted to absorption coefficient $b_{abs}(\lambda)$, when accounting for the multiple scattering effects caused by the filter and/or by the sampled particles, together with the filter loading effects that the latter are causing. Due to a lack of a reference method for providing the aerosol absorption coefficient and because every manufacturer is using different filter materials, several empirical corrections have been proposed in the literature (e.g. Weingartner et al., 2003; Virkkula et al., 2005; Collaud Coen et al., 2010; Ogren, 2010; Drinovec et al., 2015). For instance, many studies reporting absorption measurements have been calculating $b_{abs}(\lambda)$ based on Eq. 3 (Weingarter at al., 2003):

$$b_{abs}(\lambda) = \frac{b_{atn}(\lambda)}{C \cdot R(ATN(\lambda))} \quad \textbf{Eq. 3}$$

where C is the optical enhancement factor due to multiple scattering within the filter medium and $R(ATN(\lambda))$ describes nonlinearities caused by the particles loaded on the filter. Other absorption monitor manufacturers are using different approaches for deriving $b_{abs}(\lambda)$, which can be found in sections 2.2.2 and 2.2.3 for the instruments used in this study.

The equivalent black carbon (eBC) mass concentration (expressed in µg m^{-3}) can be calculated based on 880 nm wavelength $b_{atn}(\lambda)$ (Ramachandran and Rajesh, 2007), using either Eq. 4 or 5,

$$eBC = \frac{b_{atn}(880nm)}{\sigma_{atn}(880nm)} \quad \textbf{Eq. 4}$$

$$eBC = \frac{b_{abs}(880nm)}{MAC(880nm)} \quad \textbf{Eq. 5}$$

where $\sigma_{atn}(\lambda)$ is the mass attenuation cross-section and MAC, the mass absorption cross-section. Table 2 summarizes C and $\sigma_{atn}(\lambda)$ factors used for each instrument in this study. Based on these two parameters MAC can also be calculated by combining Eq. 3, 4 and 5. In this work, the term eBC was chosen instead of BC (Petzold et al., 2013) to stress that BC mass concentration is calculated from optical measurements.

Factor C is considered to be constant during each campaign as it is, relevant to the filter tape only, while R is unity for an unloaded filter and reduces when particles are deposited onto the filter (Weingarter at al., 2003). ~~Other absorption monitor manufacturers are using different approaches for deriving $b_{abs}(\lambda)$, which can be found in sections 3.2.2 and 3.2.3 for the instruments used in this study.~~ The filter strip of the miniaturized instruments evaluated in this study~~,~~ is changed manually before every flight ~~so~~ to keep the attenuation during a single flight~~the mission~~ below a threshold

value of ATN<0.1 to 0.2, above~~10-20% for~~ which loading correction is ~~not~~ required (Weingartner et al., 2003; Ferrero et al., 2011).

2~~3~~.2.2 Ground-based (reference) instruments (AE33, MAAP)

To overcome the filter loading effect discussed previously, Drinovec et al. (2015) developed the "dual spot" aethalometer (Magee Scientific, model AE33), which uses two sample spots where particles are deposited with different flow rates and one 'blank' spot as reference. The principle idea behind this approach is that any artefact~~artifact~~ induced by the accumulation of the particles onto the filter will have the same characteristics (i.e., both sample spots are probing the same particles) but the magnitude of saturation on each spot will differ due to the different amount of the sample on each respective spot.~~.~~ By combining the results from both sample spots, the measurements are extrapolated to zero loading and the compensated/corrected *eBC* mass and light absorption can be obtained without using any assumptions on the physicochemical properties of the measured particles.

Another approach for reducing the measuring biases in particle absorption coefficient induced by the accumulation of particles collected on the filter sample spot is employed by the Multiangle Absorption Photometer (MAAP) instrument (Thermo Fisher Scientific), which applies corrections on the measured~~measures~~ absorption coefficient~~of the collected particles and corrects it~~ based on the sample-laden particles'~~their~~ scattering at different angles (Petzold and Schönlinner, 2004).

In this study, these two commercially available absorption monitors (Magee Scientific - Model AE33; Thermo Scientific Fisher - Multi -Angle Absorption Photometer Model 5012) were used as a ground-based reference for UAS-based absorption measurements. Nominally MAAP measurements, which have been shown to agree well against other~~reference~~ methods (Sheridan et al., 2005), were used after being corrected based on Eq. 6 (Müller et al., 2011).~~6 (Muller et al., 2011).~~

$$b_{abs}(637) = 1.05 MAC_{BC}^{MAAP} \cdot eBC \qquad \textbf{Eq. 6}$$

where $b_{abs}(637)$ is the absorption coefficient at 637 nm (expressed in Mm^{-1}), MAC_{BC}^{MAAP} the specific mass absorption coefficient of black carbon proposed by the MAAP manufacturer equal to 6.6 m^2 g^{-1} (Petzold and Schönlinner, 2004)and *eBC* the equivalent mass concentration of black carbon reported by the instrument (in $\mu g\ m^{-3}$). Equation 6 assumes that the MAAP operates at a nominal wavelength of 637 nm as measured by Muller et al. (2011), and ~~MAAP operates~~ not at 670 nm, as proposed by the manufacturer.~~, but at 637 nm as measured by Muller et al. (2011).~~

The absorption coefficient at wavelengths different than 637 nm~~637nm~~ was calculated based on the Ångström~~Angstrom~~ law (Eq. 7).

$$\tau(\lambda) = \tau(\lambda_0)\left(\frac{\lambda}{\lambda_0}\right)^{-\alpha} \qquad \textbf{Eq. 7}$$

where $\tau(\lambda)$ and $\tau(\lambda_0)$ are the calculated and reference absorption parameters, respectively and α is the absorption Ångström~~angstrom~~ exponent (AAE). ~~.~~The reported *eBC* measurements of AE33 were used to calculate $b_{atn}(\lambda)$ and $b_{abs}(\lambda)$ based on Eq. 3 and 4 and using values of mass attenuation cross-section and optical enhancement factor reported in the literature (Table 2). In this work, the absorption coefficient calculated by the AE33 will be scaled to match measurements from MAAP. For the MAAP

instrument, the reference absorption (λ_0) is at 637 nm, as suggested by~~the one based on~~ Eq. 6 ~~at 637nm~~. The Ångström~~angstrom~~ exponent was calculated by linear regression of the natural logarithm of the seven wavelength absorption coefficients measured by AE33 (370, 470, 520, 590, 660, 880 and 950 nm) and used for extrapolating into shorter and longer wavelengths of the absorption coefficients measured by the MAAP. ~~The reported *eBC* measurements of AE33 were used to calculate $b_{atn}(\lambda)$ and $b_{abs}(\lambda)$ based on Eq. 3 and 4 and using values of mass attenuation cross section and optical enhancement factor reported in the literature (Table 2).~~ Loading correction was not applied to the AE33 measurements as it incorporates a loading compensation measurement scheme (Drinovec et al., 2015).

The AE33 was always operated at a 1 min time resolution; the MAAP operated at a 30 min time resolution during the Athens campaign and at a higher (2 min) time resolution during the Cyprus~~CAO~~ campaign.

~~2During both campaigns lidar measurements at 532 nm from the EARLINET PollyXT-NOA system, described by Engelmann et al., 2016, was used to detect the PBL depth. During the Athens campaign, measurements were collocated with the in-situ measurements described above. During the Cyprus campaign, the PollyXT measurements were located 21 km east of the ground based measurements. Nevertheless, spatiotemporal homogeneity has been observed between the two sites for that specific period (Mamali et al., 2018; Marinou et al., 2018). The PollyXT lidar quicklooks from both campaigns can be found online (http://polly.tropos.de).~~

~~3~~.2.3 Miniature Absorption Monitors (AE51, DWP, STAP)

Three miniaturized instruments having optimal specifications to fly onboard UAS were evaluated. They consist of 1) a single wavelength commercially available absorption monitor (Aethlabs, Model AE51), 2) a Dual Wavelength Prototype (DWP) monitor based on the AE51 ~~model~~ concept, and 3) a Single channel Tricolor Absorption Photometer (STAP; Brechtel Inc - Model 9406). These three~~3~~ instruments will be referred to ~~in the following~~ as AE51, DWP and STAP, respectively, in the following sections. Table 3 summarizes the characteristics of each monitor.

The AE51 is the lightest instrument (280~~150~~ g) which is a major asset for small UAS observations. On the other hand, ~~and~~ due to a relatively low air sampling flow rate (0.1-0.2 L min^{-1} set by the user), it may lack sensitivity for low concentrations of absorbing aerosols~~material~~ which can be an issue when investigating the low amounts of aerosols usually met aloft.~~in the free troposphere.~~ The two other instruments (DWP and STAP) have ~~a~~ higher flow rates~~rate~~ (2 and 1.3 L min^{-1}, respectively) which may improve sensitivity for low concentrations. These two instruments ~~have~~ also have the potential to derive additional information regarding absorbing material (other than black carbon) using the Aethalometer model reported by Sandradewi et al. (2008). On the other hand, they are significantly heavier (660 g and 1.1 kg for STAP and DWP, respectively) which may represent a major constrain for small UAS operations. The DWP has been constructed as a modification of the AE51, by placing an additional light source, emitting at 370 nm. Additionally, the sampling flow rate has been increased to 2 L min^{-1}, by replacing the original ~~UAS flights.~~AE51 pump, with an external whose flow rate is controlled by a critical orifice. The external pump resulted in additional weight to

DWP. In order to assess the possible impact of changes in relative humidity on the attenuation measurements, a second DWP monitor was installed in series behind the one which is been evaluated here. The hypothesis here is that both DWP should be similarly affected by artifacts induced by water absorption/desorption onto the filter strips. An underlying assumption is that both monitors were operating under the same temperature. Under normal (dry) conditions, the second DWP should always report zero concentrations.

The STAP,~~The STAP (Single-channel Tri-color Absorption Photometer, Brechtel Model 9406),~~ formerly named ABS (see Bates et al., 2013) has been manufactured following the design of the Particle Soot Absorption Photometer (PSAP; Bond et al., 1999)~~Bond et al., 1999)~~, except that the detection electronics have~~has~~ been completely redesigned to significantly improve signal-to-noise and provide a detection limit of ~0.2 Mm^{-1}. Light from three LED sources with wavelengths centered at 445, 515 and 633 nm (Table 3) is alternatively transmitted through glass windows with 50 Hz frequency. The diffused light, which is transmitted through two filter-holding spots that typically carry glass fiber filters, is continuously monitored by two photodetectors. One filter spot is only loaded with the sample aerosol while the other remains sample-free, acting as a reference. The highest measurement~~sampling~~ rate achieved is 1 Hz. The glass fiber filters minimize light from being transmitted in the forward direction (forward scattering) thus reducing the bias due to scattering by the collected aerosol, while they allow the sampled particles to be embedded within the filter, integrating them in the optically diffusive environment. A laminar flow element is used to measure the sample volumetric flow rate in real -time and an on-board software automatically controls the small integrated vacuum pump to maintain a constant sample volume flow independent of the UAV altitude. The sample flow is dried to eliminate artifacts due to water uptake by the filters.

Calculated absorption from the 3 miniature instruments was derived directly from the sample and reference signals, using Eq 1, 2 and 3 without taking into account the computed *eBC* or $b_{atn}(\lambda)$ reported by the instruments. For AE51 and DWP, the difference between the calculated and reported absorption values was 0.01% or less. The $b_{atn}(\lambda)$ reported by STAP was initially processed with a 60 s moving average which was deemed too long. To address that issue, a custom-made moving average was applied to the raw (1 Hz~~1Hz~~ time resolution) $b_{abs}(\lambda)$ signal in order to reduce the signal-to-noise ratio (more details in Section 4). Furthermore, this custom moving average allowed a more accurate determination of $b_{abs}(370)$ and $b_{abs}(880)$ based on Eq. 7 for STAP. The STAP manufacturer suggests conversion from $b_{atn}(\lambda)$ to $b_{abs}(\lambda)$ based on Eq. 8 (Ogren et al., 2010), which also accounts for loading artifacts. This conversion has been applied explicitly~~only~~ on STAP measurements instead of Eq. 3 (which has been applied to other miniature absorption monitors).~~3.~~

$$b_{abs}(\lambda) = \frac{0.85 b_{atn}(\lambda)}{1.22(1.0796\frac{\mathrm{I}(t)}{I_{wf}} + 0.71)} \qquad \text{Eq. 8}$$

Here,~~where~~ $I(t)$ is the attenuation at a given time (t) and I_{wf} the measured attenuation of a clean and new filter under particle -free air.

3. Sampling Sites

Sampling was conducted at two contrasting locations in the Eastern Mediterranean basin; an urban site (Athens, Greece) for a 1-week intensive period starting from 14 January 2016 and a background location in Cyprus for a 1-month intensive campaign in April 2016.

3.1 The Athens campaign

In the framework of the European project ACTRIS 2 (Aerosols, Clouds, and Trace Gases Research Infrastructure), three miniaturized absorption instruments were tested and intercompared for a period of one week (14-21 January 2016) onboard a multicopter over Athens, a city highly impacted by strong UV absorbing domestic heating biomass burning aerosols during winter (Florou et al., 2017; Fourtziou et al., 2017). Flights were conducted at Lofos Nymphon (37°58'19.68"N - 23°43'5.32"E) situated at the historical center of Athens, a metropolitan area of more than 4,000,000 inhabitants. Lofos Nymphon is a rock plateau inside a small forested area (Fig. 2), at a 50 m elevation from its surroundings. Traffic roads, marked with red lines in Fig. 2, are located westerly of the site, the closest of which is 150 m away from the measurement site. In order to comply with air space restrictions made by the Hellenic civil aviation authorities at Lofos Nymphon, the multicopter, described in detail in Section 2.1.3, was selected for its capacity to take-off and land vertically.

A total of 26 flights were performed during periods without precipitation or strong winds. Each flight lasted for 15min and reached as high as 1 km a.s.l. in altitude, a limit set by the Hellenic civil aviation authorities.

During this campaign, the flight plan has been elaborated as the following: two early morning flights were performed at an interval of c.a. one hour starting at sunrise (05:00 UTC) to investigate the stratification of the atmosphere (boundary layer, low free troposphere). Two late afternoon flights ending approximately at sunset (16:00 UTC) were performed to investigate the vertical mixing of urban emissions in the atmospheric column. On 19 January 2016, intensive (hourly) flights were performed to investigate the impact of the diurnal development of the boundary layer on the vertical distribution of absorbing aerosols. These flights are further discussed in Section 7.

Due to payload restrictions (2 kg maximum for scientific instrumentation and another 2 kg payload for the batteries, dryer, and inlet), not all the miniature monitors could fly simultaneously on board the multicopter. The monitors that could not fly, were operated at the co-located National Observatory monitoring station at Lofos Nymphon, together with two commercially available instruments (AE33; MAAP). In addition, the absorption monitor on board the multi-copter was set to measure at ground level for 2-3 min before and after each flight for a direct comparison against ground-based instruments.~~changing the filter medium.~~

3.2 The Cyprus campaign

In the framework of the European project BACCHUS (Impact of Biogenic versus Anthropogenic emissions on Clouds and Climate; towards a Holistic UnderStanding) a 1-month campaign (30 March - 28 April 2016) was performed at the Cyprus Atmospheric Observatory (CAO, 35° 2'17.97"N - 33° 3'28.50"E), a remote regional background site at the Agia Marina Xyliatou in Cyprus.

Vertical profiles of aerosol absorption were performed above a dedicated UAS airfield (35° 5'41.93"N - 33° 4'54.26"E) located at approximately 7 km north of the CAO (Fig. 2). The airfield, shown in Fig. 1, is associated with a 500 m radius (in the x-y plane) UAS airspace and an additional 500 m radius buffer zone, yielding a total of 1 km radius flight zone granted by the Cypriot civil aviation authorities and extending up to a height of approximately 2.4 km a.g.l. (2.7 km a.s.l.).

In this work, only the absorption measurements will be examined corresponding to a total of 17 flights performed with the Skywalker X8 and 6 flights with the Cruiser. The UAS flight strategy was designed to characterize the boundary layer and free troposphere with respect to aerosol absorption, number size distribution, and ice nuclei (IN) concentrations (see Schrod et al., 2017). The typical UAS flight period usually spanned from sunrise (05:00 UTC) to 09:00 UTC. Two types of fixed-wing UASs were used during this campaign; two Skywalker UAS (Model X8) and one Cruiser UAS (see section 2.1). Skywalker X8 flights typically lasted 30 min, while each Cruiser flight lasted between 1-1.5 h. Vertical profiles were performed almost on a daily basis provided meteorological conditions were favorable and engaged a team of eight persons (two pilots, two ground control station operators, two electronic/mechanical engineers and two scientific staff for the operation of the miniaturized instruments).

Ground-based absorption measurements were conducted in parallel at CAO using two commercially available instruments (AE33 and MAAP, see section 2.2.2). CAO is located 6.74 km southerly and at a 200 m elevation from the airfield (Fig. 2). Because of no significant local contamination sources in the surrounding area (Kleanthous et al., 2014; Pikridas et al., 2018), it has been assumed that the atmospheric composition at CAO and the UAS airfield were similar, allowing a direct comparison between the ground and airborne measurements. During this campaign, regional dust transport originating from Africa was identified on two occasions: 9 and 20 April 2016 (Schrod et al., 2017).

During both campaigns lidar measurements at 532 nm from the EARLINET PollyXT-NOA system, described by Engelmann et al., (2016), were used to detect the PBL depth. During the Athens campaign, measurements were collocated with the in-situ measurements described in Section 2.2.2. During the Cyprus campaign, the PollyXT measurements were located 21 km east of the ground-based measurements. Nevertheless, spatiotemporal homogeneity has been observed between the two sites for that specific period (Mamali et al., 2018; Marinou et al., 2018). The PollyXT lidar quick looks from both campaigns can be found online (http://polly.tropos.de).

4. Data exploitation: Improvement of the Optimized Noise-reduction Averaging (ONA) Smoothing Algorithm

The three miniature absorption monitors were set to sample at a rate of 1 Hz. However, all measurements were subjected to non-negligible instrumental noise (defined as one single standard deviation of the absorption coefficient) making the data exploitation for short time intervals challenging. The use of a standard averaging method (average, rolling average, least -squares fit) would require setting a fixed time step duringupon which all measurements will be averaged regardless of the signal-to-noise ratio. This will reduceresult to reduced noise but may compromise the need for

high time (spatial) resolution requiredas it is the case for UAS-based vertical profile measurements. Instead, Hagler et al.,. (2011) proposed a method where the averaging step is not defined by the time, but is based on the measured attenuation. In that method, named Optimized Noise-reduction Averaging (ONA), *dATN(λ)/dt* should only be positive or zero (but not negative, an assumption which is valid in our case without any fresh volatile sample fraction).). As a result, for a predefined configuration (sample volume, sample spot area), the same averaging attenuation step (ΔATN) will require more data points to be averaged during periods with low atmospheric concentrations (i.e lower time resolution) compared to periods with high atmospheric concentrations. Therefore, using ONA, the averaging time step is dynamically set to be inversely proportional to the sampled concentration (see also Eq. 2), resulting in a fixed signal-to-noise ratio.2). Since the method is based on attenuation changes, it can only be applied to individual spots, where the sample is accumulated, in a continuous monitor or an individual filter in semi-continuous monitors such as the miniature absorption monitors investigated in this work.

The algorithm proposed by Hagler et al. (2011) results in an integrated-like (fragmented) data structure which significant lowers the vertical resolution of our UAS-based absorption measurements significantly (blue dots in Fig. 3). To cope with this issue, an improvement of the ONA Additionally the algorithm is proposed here. A moving average is implemented instead of the one applied in the ONA algorithm, resulting in a more continuous-like data structure and improved vertical resolution (red dots in Fig. 3). If more than one wavelength is monitored, then the improved ONA algorithm can be applied to each of the wavelengths but based onassumes that the same attenuation, in order to produce comparable averaging results. The same strategy can be applied to external datasets step will be used for comparison purposes, provided they are produced or conditioned to have the exact same time resolution. each wavelength independently of the fact that attenuation of shorter wavelengths usually progresses faster.

To cope with the above issues, an improvement of the ONA algorithm is proposed here. A moving average is implemented instead of the one applied in the ONA algorithm, resulting in a more continuous-like data structure and improved vertical resolution (red dots in Fig. 3). If more than one wavelength is monitored, then the improved ONA algorithm is applied to all wavelengths but based on the attenuation of the larger one, so to produce comparable averaging results.

The flow diagram of the proposed improved ONA algorithm is presented in Suppl. Fig. 1. A link to the actual code is also provided, via a file -sharing portal, in the supplement. The user supplies attenuation, and instrument response (e.g. *eBC* mass, b_{abs}, or an external measurement) as time series along with the desired attenuation step (ΔATN). If more than one wavelength is to be examined, they have to be specified. Initially, the longer wavelength is automatically selected and a time interval based on the desired ΔATN value is calculated for each data point. The calculated time interval includes attenuation values in the range [-0.5×ΔATN, + 0.5×ΔATN] centered at the selected data point. If the attenuation change of a data point is greater by 0.5×ΔATN with respect to its neighbors, then this data point will not be smoothed. The time interval is limited to correspond to only one sample spot. The same averaging times can beare then applied to the remaining monitored wavelengths, if any. Discrepancies could arise

when abrupt concentration gradients are sampled e.g monitoring the vertical profile of a polluted boundary layer followed by clean air masses. In this case, the rate of attenuation change will decrease, since the air mass contains less absorbing aerosol. If the concentration gradient between the two layers is large enough the algorithm may lead to a fictitious shift of the boundary layer height because more data points from the clean air mass than the polluted boundary layer will be accounted for in the average. The discrepancy is solved if weights inversely proportional to the number of data points are used for the average before (-0.5×ΔATN) and after (+ 0.5×ΔATN) the sample point to be examined ~~are applied~~. The improved ONA algorithm incorporates filters that cope with this problem. Erroneous results may also arise from outliers in the time series, especially if small ΔATN is~~are~~ applied or if the time series is over smoothed.~~are oversmoothed.~~ An example of over smoothing~~oversmoothing~~ is shown in Fig.3 (green line~~dots~~). For all the reasons discussed above, it is advised to examine the result using different ΔATN and against the raw input.

High ΔATN values will reduce noise but reduce the time (vertical) resolution. A ΔATN equal to 0.01, 0.03, 0.03 is suggested for AE51, DWP and STAP, respectively, and these values take into account the air face velocity set for each instrument. Vertical profile case studies are therefore discussed later in Section 7~~6~~ with the above -proposed attenuation steps. Note that Hagler et al. (2011) suggests a higher ΔATN, equal to 0.05, for all monitors regardless of individual face velocity.

5. Quality Assurance

Despite that all the available methods have the scope of reporting the mass concentration of BC, discrepancies between the different techniques or even instruments that are based on the same operating principles have been reported (eg., Watson et al., 2005; Slowik et al., 2007; Müller et al., 2011). These discrepancies are not only attributed to the different measurement techniques/instruments used but also to the large variability of the physicochemical properties of atmospheric or laboratory-generated carbonaceous particles. For instance, the optical properties of carbonaceous particles depend on their size and morphology (Bond and Bergstrom, 2006; García Fernández et al., 2015), on their mixing state and/or coating thickness with other atmospheric relevant species, including sulfate, water, organic or dust (Lack and Cappa, 2010; Shiraiwa et al., 2010; Lack et al., 2014; Liu et al., 2015; Zhang et al., 2015, 2018) As a result, aerosol absorption measurements need to be associated with a comprehensive understanding of the methods and uncertainties associated with each instrument and how they have been operating and operated in the field. Condensation or volatilization of water on the filter spot of the miniature sensors can greatly affect absorption measurements (Hale and Querry, 1972; Düsing et al., 2019). In order to minimize this artifact, a custom-built (lightweight) silica-gel dryer was installed at the inlet of each miniature sensor and regenerated before each flight. Each sensor operated with its own respective inlet and dryer during both campaigns and even when two sensors were airborne simultaneously in one UAS. However, to reduce weight, no size-selective inlet was employed. Ground-based sensors were similarly configured, at least when UAS flights were ongoing.

In the following sections, the level of agreement, at the 95% confidence interval (CI) between standard (rack) size absorption monitors and miniature absorption sensors will

be evaluated using an adaptation of the standard Student's t-test (Welch, 1947) that accounts for samples with unequal variances and unequal sample sizes. Because the test is valid only for normal distributions the datasets to be compared are transformed (e.g. Box Cox transformation) and tested by an F-test (Box, 1953) to satisfy this assumption.

5.1 Aerosol Absorption derived by AE33 and MAAP

During the Athens campaign AE33 and MAAP showed excellent correlation (R^2=0.98, N=381) with respect to the *eBC* mass concentration trend at a 30 min time resolution (Fig. 4). However, AE33 reported higher eBC by 20±11% compared to MAAP, and higher absorption coefficient at 370, 637 and 880 nm of more than a factor 2. Each of these differences isare statistically significant at the 95% ~~confidence interval (~~CI.~~).~~ During the Cyprus campaign, ~~the~~ both monitors also showed a very good correlation (R^2=0.89, N=1434) at a 30 min time resolution. However, similar to the Athens campaign, AE33 showed *eBC* mass concentration higher by 13±5% ~~higher~~ compared to MAAP, and higher absorption coefficient at 370, 637 and 880 nm by almost a factor 2, which was also significant at 95% CI. It is noted that for both campaigns the absorption coefficient has been derived from *eBC* for both instruments. The large difference observed concerning the absorption coefficient is due to the different generic *MAC* values applied to each instrument. As an example, the *MAC* value employed by MAAP is equal to 6.6 m^2 g^{-1} at 637 nm (Table 4), while the *MAC(637)* calculated for AE33 is equal to 10.7 m^2 g^{-1}. For both campaigns, the comparison of *eBC* and the absorption coefficient at 370 and 880 nm is shown in Fig. 4, and for the absorption coefficient at 637 nm at Suppl. Fig. 2.

Drinovec et al. (2015) suggested that AE33 could overestimate *eBC* up to approximately 7% when compared to MAAP. MüllerMuller et al. (2011) calculated the absorption coefficient at 637 nm of single spot aethalometers measuring ambient air and showed that it can be up to 60±20% overestimated when compared to MAAP. Finally, MAAP has been reported to underestimate *eBC* in polluted environments (Hyvärinen et al., 2013) when the measured *eBC* concentration exceeds 3 μg m^{-3}. Table 4 summarizes the results from both campaigns (illustrated in Fig 4). ThisClearly, this comparison suggests that AE33 and MAAP exhibit a better match with respect to *eBC* mass rather than with the absorption coefficient.

In the comparison presented above, MAAP was chosen as the reference instrument because it has been shown to exhibit good agreement against ambient absorption methods (Sheridan et al., 2005) that do not require correction schemes (e.g. photoacoustic spectrometers) and because its unit-to-unit variability reported to be small (approximately 5%; MüllerMuller et al., 2011). However, MAAP monitors absorption at a single wavelength and samples at lower temporal resolution than the one desired for this study (30 min in the Athens campaign and 2 min in the Cyprus campaign).

In the following sections, we investigate how measurements from miniature attenuation monitors relate to the commercial ones discussed in this section. AE33 is always utilized as a reference because of its high temporal resolution (1 min). For this purpose, AE33 results are first scaled to match those of MAAP, to approximate, at least on average, the suggested "reference" values taking advantage of the excellent trend agreement between these two instruments. The *eBC* by the AE33 was consequently

decreased by 20% and 13%. The difference in the scaling factor between the two campaigns is attributed to instrument variability since two different pairs (of AE33 and MAAP) were employed in each campaign and to the different aerosol sampled, fresh vs aged during the Athens and Cyprus campaigns, respectively. Consequently,%, b_{abs}(370) was decreased by a factor of 2.4 and 1.93, and b_{abs}(880) was decreased by a factor of 2.2 and 1.83 during the Athens and CyprusCAO campaigns, respectively.

5.2 UAS-based absorption measurements

The loading correction term in Eq. 3 was neglected in our study, assuming a value equal to unity when attenuation was low. It is noted that currently, most loading correction schemes are applied to continuous monitors that change sample spots automatically. Attenuation of AE51, provided by the instrument never exceeded 0.011% during the Athens campaign due to the combination of low sampling flow rate and limited sampling times (approximately 15 min) of each flight. During the Cyprus campaign, it reached up to 0.022% because sampling time was higher (1-1.5 h) despite the lower measured *eBC* concentrations. Because of its higher sampling flow rate, the attenuation of DWP at 880 nm exceeded 0.15,%, five times in each of the two campaigns. In order to examine whether measurements by DWP exceeding 10% attenuation of 0.1 were significantly affected by the filter loading effect, a comparison with respect to b_{abs}*(880)* was conducted against both AE51 and AE33. The comparison results, shown in the supplementary material (Suppl. Fig. 32), support the assumption of a loading correction (*R*) equal to unity was valid during both campaigns (as already discussed by Weingartner et al., 2003).

As discussed in Section 2.2.3, the A second DWP configuration consisted of two monitors samplingmonitor was installed in series, behind the one which is been evaluated here in order to assess the possible impact of changes in relative humidityRelative Humidity on the attenuation measurements. The second DWP was measuring signals downstream of the filter strip of the DWP; the hypothesis here is that both DWP should be similarly affected by artifacts induced by water absorption/desorption onto the filter strips. An underlying assumption is that both monitors were operating under the same temperature. Under normal (dry) conditions, the second DWP should always report zero concentrations; this was the case during the Athens campaign with the exception of one flight performed on the 15th January 2016 when the silica gel dryer was removed. During this flight, the second DWP provided attenuation measurements deviating from zero, as high as 30 Mm^{-1} at 880 nm, suggesting that the first DWP measurements may also have been affected by sampling bias (Suppl. Fig. during this particular flight (Suppl. Fig. 4). Recently, Düsing et al. (2019) evaluated the discrepancy due to RH gradients of STAP to be 10.08 Mm^{-1} s^{-1} for every 1% change in RH. 3).

6. Comparison of miniature attenuation monitors against reference instruments

Since most of the commercially available sensors provide BC readings (instead of absorption like STAP), we have decided to extend our absorption intercomparison to *eBC*. Despite BC being the most absorbing material in ambient air, other components, such as brown carbon and dust could also contribute to absorption especially at shorter wavelengths (Andreae and Gelencsér, 2006).Despite BC being the most absorbing

~~material in ambient air, others components, such as brown carbon and dust could also contribute especially at shorter wavelenghts (Andreae et al., 2006). In this work, the term *e*BC was chosen instead of BC (Petzold et al. 2013) to stress that BC in not the only absorbing material.~~ In addition to *eBC*, aerosol absorption coefficients at 370 and 880 nm were also selected because two of the three miniaturized sensors measured at least at one of those wavelengths (see Table 3). Extrapolation based on Ångström~~angstrom~~ law (Eq. 7) was applied for STAP~~the monitors~~ that did not measure at these two specific wavelengths using as a base the 445 nm and the 633 nm channels to convert to 370 nm and 880 nm, respectively.

6.1 Overview of the temporal and diurnal variability of ground-based *eBC* during the Athens and Cyprus campaigns

During the Athens campaign, the average *eBC* concentration determined by AE33 was 1.5±2.1 μg m^{-3}, ranging from 0.3 to 15 μg m^{-3}. The presence of BC from biomass burning (BC_{bb}), was identified and quantified throughout the campaign (Suppl. Fig. 5), using the Sandradewi et al. (2008) model, but never exceeded 20% of the total *eBC* during daytime (05:00-15:00). During the nighttime, BC_{bb} concentration was always elevated, reaching 40-60% of the total *eBC* that typically remained below 2 μg m^{-3}. On two occasions (14 Jan 16:00 – 15 Jan 05:00 and 21 Jan 15:00 – 22 Jan 00:00) *eBC* exceeded 5 μg m^{-3} for several hours dominated by BC_{bb}. On average, BC_{bb} was identified from 16:00 UTC till 04:00 UTC of the following day and was more prominent during the periods featuring a low boundary layer and the need for heating due to low temperatures. Similar behavior attributed to biomass burning aerosol has been reported previously in Athens (Florou et al., 2017; Fourtziou et al., 2017) and other major Greek cities (Petrakakis et al., 2013; Pikridas et al., 2013). BC related to fossil fuel also exhibited a distinct diurnal pattern that included two maxima (Suppl. Fig 5). The first was observed approximately 06:00 UTC that was attributed to the rush hour traffic period and the second in late afternoon/evening (after 16:00 UTC) simultaneously with the period when biomass burning related BC was observed. Increased biomass burning, especially during nighttime for domestic heating purposes, due to the economic crisis in Greece, has been reported for another major Greek city (Saffari et al., 2013).

During the Cyprus campaign,~~During the Cyprus campaign~~ *eBC* measured by AE33 did not exceed 2 μg m^{-3} and most of the time it was found below 0.8 μg m^{-3}. The highest hourly concentration (1.9 μg m^{-3}) was observed on the 10~~10~~th April 2016 (Suppl~~Supp~~. Fig. 6~~5~~) when the site was influenced by air masses from N. Africa, and the lowest (<0.1 μg m^{-3}) on the 12 and 14~~14~~th of April 2016. During the Cyprus campaign, dust transport from the Saharan desert was identified on 3 occasions (7-10, 15-17 and 21-27 April 2016) based on combined information from i) elevated coarse-mode particulate matter concentrations measured by a tapered element oscillating microbalance (Thermo model 1400a),~~,~~ ii) aerosol spectral properties of the entire atmospheric column measured by sun photometry~~ and~~ iii) back-trajectory analysis and iv) satellite pictures (MODIS AOD product). The diurnal pattern of *eBC* during the Cyprus campaign was relatively flat as expected in a remote background site, characterized by an almost invariable concentration approximately at 0.4 μg m^{-3} (campaign average equal to 0.39±0.24 μg m^{-3}).

6.2 Ground-based intercomparison of aerosol absorption

During the Athens campaign, each miniature sensor not performing vertical profiling~~,~~ was operating at ground level in parallel with AE33 and MAAP, allowing a direct comparison. Additionally, the miniature sensors on -board the multi-copter were measuring at ground level (2-3 min) before take-off and after landing. It is noted that the same setup (sampling lines, diffusion dryer) was utilized whether the miniature samples were mounted in the UAS platform or not. Based on the combination of these datasets resampled to 1 min (the time resolution of AE33), DWP exhibited good correlation, with respect to *eBC* against AE33 (R^2=0.90, slope=0.93, N=417) shown in Fig. 5a, while the AE51 producedperformed slightly poorer correlation (R^2=0.76, slope=0.94, N=125) (see Table 4). One possible explanation is the lower signal-to-noise ratio of AE51. Both monitors measured *eBC* concentrations lower by 6-7% compared to the reference measurements. This difference is not statistically significant, at the 95% CI, for both DWP and AE51. STAP does not report *eBC* mass concentration and was excluded from this comparison for that purpose.

With respect to $b_{abs}(\lambda)$ at 370 and 880 nm, both STAP and DWP showed good correlation (At 370 nm : R^2=0.89 and 0.87, N=519 and 417 for STAP and DWP, respectively; At 880 nm : R^2=0.88 and 0.9, N=519 and 417 for STAP and DWP, respectively)) against AE33, while the correlation with AE51 was slightly poorer (R^2=0.76, N=125) at 880 nm (Fig. 5c).

However, DWP overestimated $b_{abs}(880)$ by 29±20% (significant at 95% CI) compared to the corresponding reference measurements, even though the *eBC* mass, calculated from the same wavelength, was underestimated by 7%. Similar to DWP, AE51 overestimated $b_{abs}(880)$ by 30±12% even though *eBC* mass was underestimated by 6%. This difference was statistically significant at 95% CI but only marginally (p-value equal to 0.049). Both DWP and AE51 share the same σ_{atn} and *C* values (Table 4). For both instruments, a generic *MAC(880)* value equal to 6.1 m^2 g^{-1} is applied to convert *eBC* to b_{abs}, instead of 7.8 m^2 g^{-1} used by AE33 at the same wavelength. However, both Both miniature sensors underestimate with respect to *eBC* but at the same time overestimate with respect to the absorption coefficient mainly due to the higher correction factor applied to the AE33 measurements concerning the latter (approximately a factor of 2) compared to the former (≈20%) to match those of MAAP as discussed in Section 5.1.

STAP was found to overestimate $b_{abs}(880)$ by 6±8.5% and underestimate $b_{abs}(370)$ by 7±7%. Both differences were not significant at 95% CI. During a laboratory comparison (MüllerMuller et al., 2011) reported that a continuous single spot aethalometer (Magee Model AE31) overestimated b_{abs} compared to MAAP by 37-60% at 660 nm. The same study also reported underestimation of the absorption coefficient at 650 and 585 nm against MAAP compared toof the Particle Soot Absorption Photometer (Radiance Research Model PSAP (,the rack -mounted equivalent of STAP) by 1-14%. These laboratory comparison results are similar to those reported in this study (AE51 overestimates and STAP underestimates the absorption coefficient by aby similar extent against the reference).

TheThese results suggest that the miniature sensors intercompared during the Athens campaign~~,~~ exhibit better agreement with respect to the parameter they report.

Concerning AE51 and DWP, this parameter was *eBC* concentration, which was within 10%, rather than the absorption coefficient, suggesting that the absorption coefficient should be preferentially calculated based on a single set of wavelength-dependent MAC values (Eq. 5) instead~~,~~ if these are known or can be calculated. On the other hand, STAP that does not report *eBC* but b_{abs} exhibited good agreement, within 10%, against the reference on that property. On~~The discrepancies discussed above lead to an~~ average ~~underestimation in~~ the calculated AAE~~angstrom exponent~~ of DWP and STAP is underestimated~~against that of AE33~~ by 13% and 12% respectively against that of AE33.

During the Cyprus campaign, aerosol absorption was also monitored at the ground by an AE33 and a MAAP located at CAO, approximately 7 km away and at 200 m higher elevation from the UAS airfield. Only DWP and AE51 were used on UAS during this campaign. Assuming homogeneity between the two sites, a direct comparison was conducted between ground and UAS measurements.

The comparison results, shown in Fig. 6, indicate that the correlation between the ground measurements and UAS (AE51 and DWP) measurements led to less satisfactory results compared to the Athens campaign (see also Table 4). The correlation between AE33 and DWP was still acceptable (R^2=0.71; N=91) with respect to *eBC* and the absorption coefficient at 370 and 880 nm at 1 min time resolution. But the correlation between AE33 and AE51 was found ~~as~~ poor (R^2=0.32, N=48) with respect to both *eBC* and $b_{abs}(880)$.

The atmospheric~~Atmospheric~~ concentration of absorbing material (~~with respect to~~ *eBC* measurements) was found on average 4 times lower in Cyprus (mean of 0.39±0.24 μg m^{-3}) compared to Athens (mean of 1.5±2.1 μg m^{-3})~~.), limiting the performance of the miniature sensors.~~ Additionally, the range of atmospheric concentrations was also reduced by a factor of 6 in Cyprus (maximum hourly averaged *eBC* was 1.9 μg m^{-3}) compared to Athens (maximum hourly averaged *eBC* was 12.2 μg m^{-3}), leading to less favorable conditions for direct instrument-by-instrument comparisons due to the smaller range of comparison data.~~.~~ These conditions had a direct impact on~~in~~ the uncertainty related to the measurement agreement between the AE33 and the miniature monitors. During the Cyprus campaign, the uncertainty was always greater than the respective of the Athens campaign. As an example during the Cyprus campaign, DWP underestimated *eBC* by 6±20% and overestimated $b_{abs}(880)$ by 20±26% (both significant at 95% CI), while during the Athens one the respective numbers were 7±15% and 29±20% (Table 4). The effect was greater concerning AE51, which overestimated *eBC* by 22±52% and $b_{abs}(880)$ by 55±66%, while during the Athens campaign the respective numbers were 6±9% and 30±12% (Table 4). Due to the large uncertainty exhibited by AE51, the null hypothesis that the population mean of the reference instrument (AE33) and of AE51 are different was not met. Hence, the reported differences are not significant at the 95% CI. It is unclear whether the absorbing properties of the sampled aerosol (fresh at Athens and aged in~~at~~ Cyprus) had any effect on this comparison.

6.3 On flight intercomparison of aerosol absorption

During flights, vibrations, as well as strong gradients of pressure, temperature, and RH may affect the performance of the miniature sensors. In order not~~Due~~ to surpass the maximum take-off~~extra~~ weight of the multicopter used during the Athens

campaignissues, STAP and DWP didcould not fly simultaneously. However, the lower weight of AE51 enabled on-flight cross -comparison with DWP and STAP, respectively during 8 flights of the Athens campaign. The correlation of AE51 airborne with both DWP and STAP was very good (R^2=0.65, N=493 and R^2=0.87, N=1875, respectively) provided that the sampled air was dried (Fig. 7) and the dataset post processed with a noise-reducing algorithmconditioned as suggested in Section 4. Error bars shown in Fig. 7 correspond to one standard error for one-second time resolution. In the case that the algorithm did not average a sampling point with its neighbors, then by default, the standard deviation and standard error were zero, indicated by a lack of an error estimate in Fig. 7. Note that, if no smoothing is applied, then the correlation deteriorates sharply (R^2=0.01) for either DWP or STAP. The ΔATN used for this comparison were 0.01, 0.03, and 0.03 for AE51, DWP, and STAP, respectively as suggested in Section 4. STAP is shown to underestimate b_{abs} by 12% (significant at 95% CI) compared to AE51 (Fig. 7), consistent with the comparison against AE33 discussed in Section 6.2. The very good correlation (comparison slope = 0.87) between the two when airborne also suggests that on average, no significant bias during the flights was present. The difference between AE51 and DWP was 8%,% which was not significant at 95% CI.

7. Diurnal Vertical Profiles of Black Carbon above Athens: A case study

As part of the Athens campaign, intensive vertical absorption profiles were performed with the objective to assess the influence of the diurnal development of the planetary boundary layer (PBL) on the vertical dispersion of ground-based black carbon emissions. UAS-based measurements were conducted for that purpose on the 1919th of January at sunrise (05:38 UTC) and were continued on an hourly basis till the PBL depth exceeded the maximum height allowed to operate (1 km a.s.l.) approximately at 10:00 UTC. Two additional flights were conducted later onin that day; one hour before and during sunset (15:38 UTC). The reconstructed vertical distribution of *eBC* based on the six ascending vertical profiles from 05:30 till 09:45 (UTC) is shown in Fig. 8, complemented by ground measurements during the same day by AE33. The actual vertical profiles for the entire day (N=8) are also shown in Fig. 9. We present a very detailed study ofTo the best of our knowledge, this is the first time that the vertical dispersion of ground-based black carbon emissions is dynamically assessed above a major city. Our results suggest a non-homogeneous boundary layer that evolved at a rate of 132 m h^{-1} during 1919th January 2016 starting from an elevation of 265 m a.s.l. before sunrise. Starting atOn the ground, *eBC* from the miniature monitor followed the diurnal pattern also observed on the ground by the reference instrument. At this low elevation and since 05:00 UTC *eBC* increased by a factor of 8, maximizing at 07:00 UTC. The emission's pattern and the Ångströmangstrom exponent, calculated based on AE33 measurements, which was equal to 1.1 when concentrations maximized, suggest that this increase in *eBC* was due to local traffic emissions (see also Fig. 8). After 10:00 UTC *eBC* remained relatively stable at 1.5 μg m^{-3} (≈5 Mm^{-1} at 880 nm).

Above the PBL, which was determined by Polly-XT measurements (Baars et al., 2008; dashed red lines in Fig. 9), the measured concentration of *eBC* was always lower than the respective one measured within, by at least 20%. The highest *eBC* concentrations above the PBL were observed during sunrise and sunset (first and last diurnal profile in Fig. 9) equal to 1.9 and 2.0 μg m^{-3}, respectively, which we interpret as the residual layer of the previous day in the morning and the newly formed residual

layer after sunset. The lowest *eBC* concentration in this layer, equal to 0.3 μg m^{-3}, was observed at 06:30 UTC but steadily increased to 0.4, 0.9 and 1.7 μg m^{-3}during 07:38, 08:39 and 09:44 UTC, respectively. Due to flight restrictions, free tropospheric measurements could not be monitored after 10:00 UTC. PBL was also identified by vertical profiles of potential temperature which are in good agreement with those derived by Polly-XT

Before sunrise, our results suggest the presence of a stable boundary layer in contact with the ground that has been radiatively cooled~~, and~~ on top of the boundary layer, there is a residual layer. As the sun rises, the stable boundary layer's depth increases and simultaneously the residual layer is mixed with the free troposphere. On~~During~~ the 19~~19~~th January 2016, mixing took place between 05:45-06:30 UTC. The concentration of *eBC* in the residual layer drops to near zero because the trapped pollutants are now diluted in the free troposphere.

However, the concentration of *eBC* above the boundary layer exhibited an increasing trend suggesting either convection of pollutants from the PBL or advection~~advections~~ of regionally transported PM involving absorbing material that did not intrude the PBL. During the period when absorbing material was directly emitted from the ground and the boundary layer height increased (from 05:30-08:30 UTC), *eBC* dispersion inside the PBL was not homogeneous but was gradually decreasing with increasing altitude. The effect is more evident when emissions from the ground exhibited an increasing trend (approximately from 06:30-07:40 UTC). Once ground emissions reached their minimum and the PBL stabilized, the concentration inside the PBL became homogeneous (from 10:00 UTC till sunset). During sunset, stratification of a new stable boundary layer was observed and on top of it a new residual layer forming.

The vertical absorption distribution was reconstructed based on the absorption profiles shown in Fig.8, on~~during~~ 19 January 2016 between 05:34 and 09:36 (UTC) and also shown in Fig. 9 against calculated attenuated backscatter at 1064 nm measured by a PollyXT~~PollyXT's range corrected signal~~.

8. Conclusions

Two field campaigns were conducted in Athens (Greece) and in CAO (Cyprus) in order to i) study the vertical distribution of aerosol absorption and ii) to evaluate the performance of three miniature absorption sensors in contrasted atmospheric environments against ground -based reference instruments (MAAP and AE33). Measurements were conducted on the ground and air using three different models of UASs. Our results suggest that the absorption monitors used in this work agree better at the parameter they report, which is *eBC* in most cases, rather than the absorption coefficient. This discrepancy is directly related to the generic *MAC* values suggested by the manufacturer of each instrument. In case the absorption coefficient is not directly reported, it should be preferentially calculated based on a single set of wavelength-dependent *MAC* values specific to each site, if these are known or can be calculated, instead of the generic provided by the manufacturer.

The influence of humidity on attenuation measurements was investigated~~UAS-based aerosol sampling was dried to minimize the influence of water absorption/desorption on the filter strips and attenuation measurements. The influence of water on attenuation measurements was confirmed~~ during the Athens campaign, by placing two DWP in

series, with the second measuring filtered air from the exhaust of the first. Sample drying minimized the influence of water adsorption/desorption on attenuation measurements.

During January 2016, the miniature sensors sampled urban aerosols at the center of Athens, Greece. On the ground, STAP and DWP followed well the observed variations in the absorption~~absorbance~~ (R^2≈0.90) against an AE33, while AE51's performance (R^2=0.76) was poorer due to low sampling flow rate. STAP~~,~~ was found to overestimate absorption coefficient at 880 nm by 10%, while AE51 and DWP overestimate it by 40% and 30%, respectively. However, with respect to *eBC* mass, the agreement was closer (within 7%). An inflight~~Taking advantage of the light weight AE51, on flight~~ intercomparison between the lightweight AE51 and either the STAP or DWP was~~could be~~ achieved during the Athens campaign~~for STAP and DWP~~. No correlation between the AE51 and STAP or DWP could be achieved for unconditioned high-time resolution (1 Hz) measurements. An improvement of the smoothing algorithm suggested by Hagler et al. (2011) was applied here leading to improved correlations (R^2>0.70) between miniature sensors (AE51, DWP and STAP). Based on four UAS flights, DWP and AE51 correlated~~agreed~~ very well (comparison slope equal to 0.92) with respect to the absorption coefficient at 880 nm ($b_{abs}(880)$), while STAP was found to underestimate $b_{abs}(880)$ by 12% which was consistent with the intercomparison performed at ground level against the AE33.

The Cyprus campaign took place at the Cyprus Atmospheric Observatory, a remote location distant by 7 km from the UAS runway and two of the miniature sensors (DWP and AE51) were evaluated in~~on~~-flight against ground-based reference instruments, taking advantage of the elevation difference between the two sites. By comparison to the Athens campaign, the correlation of both sensors (against reference instruments) deteriorated because of low atmospheric aerosol concentrations (4 times lower) and reduced atmospheric variability (6 times lower). While DWP showed relatively good correlation~~performance~~ (R^2=0.71; N=91 data points) and the same level of agreement as during the Athens campaign (6% overestimate), the poor performance of AE51 (R^2=0.32, N=91) was attributed to a lack of sensitivity of this sensor operating at a flow rate c.a. 10 times lower compared to DWP.

The overall potential use of miniature aerosol absorption sensor on-board small UAS was illustrated with results of the campaign performed in Athens. During this campaign, the diurnal variability of the vertical distribution (0-1 km a.g.l.)~~)~~ of equivalent Black Carbon was investigated. It was found that *eBC* concentrations are not homogeneous in the boundary layer when it develops (PBL depth increases) and simultaneously absorbing material is emitted at ground level by traffic. Vertical homogeneity of *eBC* is reached in the afternoon~~,~~ when the boundary layer height is stabilized and emissions at the ground are reduced.

Acknowledgments~~Acknowledgements~~: The two field campaigns (Athens, Cyprus) are a contribution to~~of~~ the ACTRIS2 project that has received funding from the European Union's Horizon 2020 research and innovation program under grant agreement no. 654109. EU FP7 project BACCHUS (project number 603445) is acknowledged for financial support. MV acknowledges support from the DFG-Research Center/Cluster of Excellence "The Ocean in the Earth System-MARUM". MP acknowledges the

financial support of the CURE-3AB project (INTERNATIONAL/OTHER/0118/0108) which is co-financed by the European Regional Development Fund and the Republic of Cyprus through the Research and Innovation Foundation. EM acknowledges the financial support of the Deutscher Akademischer Austauschdienst (grant no. 57370121), VA acknowledges the financial support of the European Research Council (grant no. 725698, D-TECT).

9. Nomenclature

Abbreviation	Description
AAE	Absorption Ångström exponent
ACTRIS	Aerosols, Clouds, and Trace Gases Research Infrastructure
a.s.l.	Above sea level
ATN	Attenuation
b_{atn}	Light attenuation~~Attenuation~~ coefficient
BACCHUS	Impact of Biogenic versus Anthropogenic emissions on Clouds and Climate; towards a Holistic UnderStanding
b_{abs}	Light absorption~~Absorption~~ coefficient
BC	Black carbon
BC_{bb}	BC related to biomass burning
C	Optical enhancement factor
CAO	Cyprus atmospheric observatory
CI	Confidence interval
DWP	Dual -wavelength prototype
EARLINET	European Aerosol Research Lidar Network
eBC	Equivalent black carbon
EC	Elemental carbon
GUI	Graphical user interface
MAAP	Multiangle Absorption Photometer
MAC	Mass absorption cross-section~~coefficient~~
MTOW	Maximum take-off weight
ONA	Optimized Noise-reduction Averaging
PBL	Planetary boundary layer
PSAP	Particle Soot Absorption Photometer
R	Filter loading parameter
STAP	Single -channel Tri-color Absorption Photometer
UAS	Unmanned aerial systems
α	Ångström~~Angstrom~~ exponent
λ	Wavelength
σ_{atn}	Mass attenuation cross -section

10. References

~~Andreae, M. O. and Gelencsér, A.: Black carbon or brown carbon? The nature of light-absorbing carbonaceous aerosols, Atmos. Chem. Phys., 6, 3131-3148, https://doi.org/10.5194/acp-6-3131-2006, 2006.~~

Andreae, M. O. and Gelencsér, A.: Black carbon or brown carbon? The nature of light-absorbing carbonaceous aerosols, Atmos. Chem. Phys., 6, 3131–3148, doi:10.5194/acpd-6-3419-2006, 2006.

Baars, H., Ansmann, A., Engelmann, R. and~~,~~ Althausen, D.~~:, 2008.~~ Continuous monitoring of the boundary-layer top with lidar~~,~~ Atmos. Chem. Phys.~~,~~ 8(23)~~,~~ 7281–7296~~, . https://~~doi~~:.org/~~10.5194/acp-8-7281-2008, 2008.

Bates, T.S., Quinn, P.K., Johnson, J.E., Corless, A., Brechtel, F.J., Stalin, S.E., Meinig, C. and~~,~~ Burkhart, J.F.~~:, 2013.~~ Measurements of atmospheric aerosol vertical distributions above Svalbard, Norway, using unmanned aerial systems (UAS)~~,).~~ Atmos. Meas. Tech.~~,~~ 6(8)~~,~~ 2115–2120~~, . https://~~doi~~:.org/~~10.5194/amt-6-2115-2013, 2013.

Bisht, D. S., Tiwari, S., Dumka, U. C., Srivastava, A. K., Safai, P. D., Ghude, S. D., Chate, D. M., Rao, P. S. P., Ali, K., Prabhakaran, T., Panickar, A. S., Soni, V. K., Attri, S. D., Tunved, P., Chakrabarty, R. K. and Hopke, P. K.: Tethered balloon-born and ground-based measurements of black carbon and particulate profiles within the lower troposphere during the foggy period in Delhi, India, Sci. Total Environ., 573, 894–905, doi:10.1016/j.scitotenv.2016.08.185, 2016.

Bond, T. C. and Bergstrom, R. W.: Light absorption by carbonaceous particles: An investigative review, Aerosol Sci. Technol., 40(1), 27–67, doi:10.1080/02786820500421521, 2006.

Bond, T. ~~Birch, M.E., Cary, R.A., 1996. Elemental Carbon-Based Method for Monitoring Occupational Exposures to Particulate Diesel Exhaust. Aerosol Sci. Technol. 25, 221–241. https://doi.org/10.1080/02786829608965393~~

~~Bond, T.~~C., Anderson, T.L. and~~,~~ Campbell, D.~~:, 1999.~~ Calibration and Intercomparison of Filter-Based Measurements of Visible Light Absorption by Aerosols~~,~~ Aerosol Sci. Technol.~~,~~ 30(6)~~,~~ 582–600~~, . https://~~doi~~:.org/~~10.1080/027868299304435, 1999.

Bond, T. C.~~,. and Bergstrom, R. W.: Light absorption by carbonaceous particles: an investigative review, *Aerosol Sci. Technol.*, 40, 27-67, DOI: 10.1080/02786820500421521, 2006.~~

~~Bond, T. C.,~~ Doherty, S. J.~~,~~ Fahey, D. W., Forster, P. M., Berntsen, T., Deangelo ~~DeAngelo~~, B. J., Flanner, M. G., Ghan, S., Kärcher, B., Koch, D., Kinne, S., Kondo, Y., Quinn, P. K., Sarofim, M. C., Schultz, M. G., Schulz, M., Venkataraman, C., Zhang, H., Zhang, S., Bellouin, N., Guttikunda, S. K., Hopke, P. K., Jacobson, M. Z., Kaiser, J. W., Klimont, Z., Lohmann, U.~~,~~ ~~J.,~~ Schwarz, J. P., Shindell, D., Storelvmo, T., Warren, S. G. and Zender, C. S.: Bounding the role of black carbon in the climate system: A scientific assessment, J. Geophys. Res. Atmos., 118(11), 5380–5552, doi:10.1002/jgrd.50171,~~ 5380-5552, doi:10.1002/jgrd.50171,~~ 2013.

Box, G. E. P.: Non- normality and tests on variances, Biometrika, 40(3–4), 318–335, doi:10.1093/biomet/40.3-4.318, 1953.

Chilinski, M. T., Markowicz, K. M. and Markowicz, J.: Observation of vertical variability of black carbon concentration in lower troposphere on campaigns in Poland, Atmos. Environ., 137, 155–170, doi:10.1016/j.atmosenv.2016.04.020, 2016.

Collaud Coen, M., Weingartner, E., Apituley, A., Ceburnis, D., Fierz-Schmidhauser, R., Flentje, H., Henzing, J. S., Jennings, S. G., Moerman, M., Petzold, A., Schmid, O.~~,~~ and Baltensperger, U.: Minimizing light absorption measurement artifacts of the Aethalometer: Evaluation~~evaluation~~ of five correction algorithms, Atmos. Meas. Tech., 3(2)~~,~~ 457–474, doi:10.5194/amt-3-457-2010, 2010.

Corrigan, C. E., Roberts, G. C., Ramana, M. V., Kim, D. and Ramanathan, V.: Capturing vertical profiles of aerosols and black carbon over the Indian Ocean using autonomous unmanned aerial vehicles, Atmos. Chem. Phys., 8(3), 737–747, doi:10.5194/acp-8-737-2008, 2008.

Drinovec, L., Močnik, G., Zotter, P., Prévôt, A.S.H., Ruckstuhl, C., Coz, E., Rupakheti, M., Sciare, J., Müller, T., Wiedensohler, A. and~~,~~ Hansen, A.D.A.~~:, 2015.~~ The "dual-spot" Aethalometer: An improved measurement of aerosol black carbon with real-time loading compensation~~,~~ Atmos. Meas. Tech.~~,~~ 8(5)~~,~~ 1965–1979~~, ~~https://~~doi:~~.org/~~10.5194/amt-8-1965-2015, 2015.

Düsing, S., Wehner, B., Müller, T., Stöcker, A. and Wiedensohler, A.: The effect of rapid relative humidity changes on fast filter-based aerosol particle light absorption measurements: uncertainties and correction schemes, Atmos. Meas. Tech. Discuss., 1–30, doi:10.5194/amt-2019-101, 2019.

Engelmann, R., Kanitz, T., Baars, H., Heese, B., Althausen, D., Skupin, A., Wandinger, U., Komppula, M., Stachlewska, I. S., Amiridis, V., Marinou, E., Mattis, I., Linné, H.~~,~~ and Ansmann, A.: The automated multiwavelength Raman polarization and water-vapor lidar PollyXT: The~~the~~ neXT generation, Atmos. Meas. Tech., 9(4)~~,~~ 1767–~~–~~1784, ~~https://~~doi:~~.org/~~10.5194/amt-9-1767-2016, 2016.

Erel, Y., Dayan, U., Rabi, R., Rudich, Y.~~,~~ and Stein, M.:~~ Tracing~~ Trans boundary transport~~ Boundary Transport~~ of pollutants~~Pollutants~~ by atmospheric mineral dust~~Mineral Dust~~, Environ. Sci. Technol., 40(9)~~,~~ 2996–3005, doi:10.1021/es051502l, 2006.

~~Fernández, C. G., Picaud, S.,~~ ~~Devel, M.: Calculations of the mass absorption cross sections for carbonaceous nanoparticles modeling soot, J. Quant. Spectrosc. Radiat.~~ ~~*Transfer*, 164, 69–81, http://dx.doi.org/10.1016/j.jqsrt.2015.05.011, 2015.~~

Ferrero, L., Mocnik, G., Ferrini, B. S., Perrone, M. G., Sangiorgi, G. and Bolzacchini, E.: Vertical profiles of aerosol absorption coefficient from micro-Aethalometer data and Mie calculation over Milan, Sci. Total Environ.~~,~~ 409(14), 2824–2837, doi:10.1016/j.scitotenv.2011.04.022, 2011.

Ferrero, L., Castelli, M., Ferrini, B. S., Moscatelli, M., Perrone, M. G., Sangiorgi, G., D'Angelo, L., Rovelli, G., Moroni, B., Scardazza, F., Mocnik, G., Bolzacchini, E., Petitta, M. and Cappelletti, D.: Impact of black carbon aerosol over Italian basin valleys: High-resolution measurements along vertical profiles, radiative forcing and heating rate, Atmos. Chem. Phys., 14(18), 9641–9664, doi:10.5194/acp-14-9641-2014, 2014.

Ferrero, L., Cappelletti, D., Busetto, M., Mazzola, M., Lupi, A., Lanconelli, C., Becagli, S., Traversi, R., Caiazzo, L., Giardi, F., Moroni, B., Crocchianti, S., Fierz, M., Mocnik, G., Sangiorgi, G., Perrone, M., Maturilli, M., Vitale, V., Udisti, R. and Bolzacchini, E.: Vertical profiles of aerosol and black carbon in the Arctic: A seasonal phenomenology along 2 years (2011-2012) of field campaigns, Atmos. Chem. Phys., 16(19), 12601–12629, doi:10.5194/acp-16-12601-2016, 2016.

Ferrero, L., Močnik, G., Cogliati, S., Gregorič, A., Colombo, R. and Bolzacchini, E.: Heating Rate of Light Absorbing Aerosols: Time-Resolved Measurements, the Role of Clouds, and Source Identification, Environ. Sci. Technol., 52(6), 3546–3555, doi:10.1021/acs.est.7b04320, 2018.

Florou, K., Papanastasiou, D.K., Pikridas, M., Kaltsonoudis, C., Louvaris, E., Gkatzelis, G.I., Patoulias, D., Mihalopoulos, N. and, Pandis, S.N.:, 2017. The contribution of wood burning and other pollution sources to wintertime organic aerosol levels in two Greek cities, Atmos. Chem. Phys., 17(4), 3145–3163, https://doi.org/10.5194/acp-17-3145-2017, 2017.

Fourtziou, L., Liakakou, E., Stavroulas, I., Theodosi, C., Zarmpas, P., Psiloglou, B., Sciare, J., Maggos, T., Bairachtari, K., Bougiatioti, A., Gerasopoulos, E., Sarda-Estève, R., Bonnaire, N. and, Mihalopoulos, N.:, 2017. Multi-tracer approach to characterize domestic wood burning in Athens (Greece) during wintertime, Atmos. Environ., 148, 89–101, https://doi.org/https://doi.org/10.1016/j.atmosenv.2016.10.011, 2017.

Freney, E. J., Sellegri, K., Canonaco, F., Colomb, A., Borbon, A., Michoud, V., Crumeyrolle, S., Amarouche, N., Bourianne, T., Gomes, L., Prevot, A. S. H., Beekmann, M. and Schwarzenböeck, A.: Characterizing the impact of urban emissions on regional aerosol particles: Airborne measurements during the MEGAPOLI experiment, Atmos. Chem. Phys., 14(3), 1397–1412, doi:10.5194/acp-14-1397-2014, 2014.

García Fernández, C., Picaud, S. and Devel, M.: Calculations of the mass absorption cross sections for carbonaceous nanoparticles modeling soot, J. Quant. Spectrosc. Radiat. Transf., 164, 69–81, doi:10.1016/j.jqsrt.2015.05.011, 2015.

Gerasopoulos, E., Koulouri, E., Kalivitis, N., Kouvarakis, G., Saarikoski, S., Mäkelä, T., Hillamo, R.Babasakalis, P., Vrekoussis, M., Putaud, J. P., and Mihalopoulos, N.: Size-segregated mass distributions of aerosols over EasternOrigin and variability of particulate matter (PM_{10}) mass concentrations over the eastern Mediterranean: Seasonal variability and comparison with AERONET columnar size-distributions, Atmos. Chem. Phys., 7(10), 2551–2561, doi:10.5194/acp-7-2551-2007, 2007, *Atmos. Environ.*, 40, 4679–4690, doi:10.1016/j.atmosenv.2006.04.020, 2006.

Hadley, O.L. and, Kirchstetter, T.W.:, 2012. Black-carbon reduction of snow albedo, Nat. Clim. Chang., 2(6), 437–440, doi:10.1038/nclimate1433, 2012.

Hagler, G.S.W., Yelverton, T.L.B., Vedantham, R., Hansen, A.D.A. and, Turner, J.R.:, 2011. Post-processing method to reduce noise while preserving high time resolution in aethalometer real-time black carbon data, Aerosol Air Qual. Res., 11(5), 539–546, https://doi.org/10.4209/aaqr.2011.05.0055, 2011.

Hale, G.M. and, Querry, M.R.:, 1972. Optical Constants of Water in the 200-nm to 200-µm Wavelength Region, Appl. Opt., 12(3), 555, https://doi.org/10.1364/ao.12.000555, 1972.

Haywood, J. and, Boucher, O.:, 2000. Estimates of the direct and indirect radiative forcing due to tropospheric aerosols: A review, Rev. Geophys., 38(4), 513–543, https://doi.org/10.1029/1999RG000078, 2000.

Höpner, F., A.-M. Bender, F., Ekman, A. M. L., Praveen, P. S., Bosch, C., Ogren, J. A., Andersson, A. and Ramanathan, V.: Vertical profiles of optical and microphysical particle properties above the northern Indian Ocean during CARDEX 2012, Atmos. Chem. Phys., 16(2), 1045–1064, doi:10.5194/acp-16-1045-2016, 2016.

Hyvärinen, A.P., Vakkari, V., Laakso, L., Hooda, R.K., Sharma, V.P., Panwar, T.S., Beukes, J.P., Van Zyl, P.G., Josipovic, M., Garland, R.M., Andreae, M.O., Pöschl,

U. and., Petzold, A.:., 2013. Correction for a measurement artifact of the Multi-Angle Absorption Photometer (MAAP) at high black carbon mass concentration levels,. Atmos. Meas. Tech.,. 6(1),, 81–90, . https://doi:.org/10.5194/amt-6-81-2013, 2013.

Inoue, Y., Morinaga, S. and Tomita, A.: A blimp-based remote sensing system for low-altitude monitoring of plant variables: A preliminary experiment for agricultural and ecological applications, Int. J. Remote Sens., 21(2), 379–385, doi:10.1080/014311600210894, 2000.

IPCC, 2013: Climate Change 2013: The Physical Science Basis. Cambridge University Press, Cambridge, United Kingdom and New York, USA, 2013.

Jensen, T., Apan, A., Young, F. and Zeller, L.: Detecting the attributes of a wheat crop using digital imagery acquired from a low-altitude platform, Comput. Electron. Agric., 59(1–2), 66–77, doi:10.1016/j.compag.2007.05.004, 2007.

Kalivitis, N., Gerasopoulos, E., Vrekoussis, M., Kouvarakis, G., Kubilay, N., Hatzianastassiou, N., Vardavas, I.., and Mihalopoulos, N.:M. Dust transport over the eastern mediterraneanMediterranean derived from total ozone mapping spectrometer, aerosol robotic networkTotal Ozone Mapping Spectrometer, Aerosol Robotic Network, and surface measurements, J. Geophys. Res. Atmos., 112(3), 1–9, D03202, doi:10.1029/2006JD007510, 2007.

Kassianov, E., Berg, L.K., Pekour, M., Barnard, J., Chand, D., Comstock, J., Flynn, C., Sedlacek, A., Shilling, J., Telg, H., Tomlinson, J., Zelenyuk, A. and., Fast, J.:., 2018. A Closure Studyclosure study of Total Scattering Using Airborne In Situ Measurementstotal scattering using airborne in situ measurements from the Winter Phasewinter phase of TCAP,. Atmosphere (Basel).,). 9(6), 228, . https://doi:.org/10.3390/atmos9060228, 2018.

Katich, J.M., Samset, B.H., Bui, T.P., Dollner, M., Froyd, K.D., Campuzano-Jost, P., Nault, B.A., Schroder, J.C., Weinzierl, B. and., Schwarz, J.P.:., 2018. Strong Contrast in Remote Black Carbon Aerosol Loadings Between the Atlantic and Pacific Basins,. J. Geophys. Res. Atmos.,. 123(23),, 13,386-13,395, . https://doi:.org/10.1029/2018JD029206, 2018.

Kleanthous, S., Vrekoussis, M., Mihalopoulos, N., Kalabokas, P. and., Lelieveld, J.:., 2014. On the temporal and spatial variation of ozone in Cyprus,. Sci. Total Environ.,. 476–477, 677–687, . https://doi:.org/10.1016/j.scitotenv.2013.12.101, 2014.

Lack, D. A. and Cappa, C. D.: Impact of brown and clear carbon on light absorption enhancement, single scatter albedo and absorption wavelength dependence of black carbon, Atmos. Chem. Phys., 10(9), 4207–4220, doi:10.5194/acp-10-4207-2010, 2010.

Lack, D. A., Moosmüller, H., McMeeking, G. R., Chakrabarty, R. K. and Baumgardner, D.: Characterizing elemental, equivalent black, and refractory black carbon aerosol particles: A review of techniques, their limitations and uncertainties, Anal. Bioanal. Chem., 406(1), 99–122, doi:10.1007/s00216-013-7402-3, 2014.

Lelieveld, J., Berresheim, H., Borrmann, S., Crutzen, P. J., Dentener, F. J., Fischer, H., Feichter, J., Flatau, P. J., Heland, J., Holzinger, R., Korrmann, R., Lawrence, M. G., Levin, Z., Markowicz, K. M., Mihalopoulos, N., Minikin, A., Ramanathan, V., De Reus, M., Roelofs, G. J., Scheeren, H. A., Sciare, J., Schlager, H., Schultz, M., Siegmund, P., Steil, B., Stephanou, E. G., Stier, P., Traub, M., Warneke, C., Williams, J. and Ziereis, H.: Global air pollution crossroads over the Mediterranean, Science (80-.)., 298(5594), 794–799, doi:10.1126/science.1075457, 2002.

Liu, D., Quennehen, B., Darbyshire, E., Allan, J. D., Williams, P. I., Taylor, J. W., J.-

B. Bauguitte, S., Flynn, M. J., Lowe, D., Gallagher, M. W., Bower, K. N., Choularton, T. W. and Coe, H.: The importance of Asia as a source of black carbon to the European Arctic during springtime 2013, Atmos. Chem. Phys., 15(20), 11537–11555, doi:10.5194/acp-15-11537-2015, 2015.

Mamali, D., Marinou, E., Sciare, J., Pikridas, M., Kokkalis, P., Kottas, M., Binietoglou, I., Tsekeri, A., Keleshis, C., Engelmann, R., Baars, H., Ansmann, A., Amiridis, V., Russchenberg, H. and., Biskos, G.:., 2018. Vertical profiles of aerosol mass concentration derived by unmanned airborne in situ and remote sensing instruments during dust events,. Atmos. Meas. Tech.,. 11(5),. 2897–2910, . https://doi:.org/10.5194/amt-11-2897-2018, 2018.

Marinou, E., Tesche, M., Nenes, A., Ansmann, A., Schrod, J., Mamali, D., Tsekeri, A., Pikridas, M., Baars, H., Engelmann, R., Voudouri, K.-A., Solomos, S., Sciare, J., Groβ, S. and., Amiridis, V.:., 2018. Retrieval of ice nucleating particle concentrations from lidar observations: Comparison with airborne in-situ measurements from UAVs,. Atmos. Chem. Phys. Discuss., (December),. 1–37, . https://doi:.org/10.5194/acp-2018-1203, 2018.

Moosmüller, H., Chakrabarty, R. K. and Arnott, W. P.: Aerosol light absorption and its measurement: A review, J. Quant. Spectrosc. Radiat. Transf., 110(11), 844–878, doi:10.1016/j.jqsrt.2009.02.035, 2009.

Müller, T., Henzing, J. S., De Leeuw, G., Wiedensohler, A., Alastuey, A., Angelov, H., Bizjak, M., Collaud Coen, M., Engström, J. E., Gruening, C., Hillamo, R., Hoffer, A., Imre, K., Ivanow, P., Jennings, G., Sun, J. Y., Kalivitis, N., Karlsson, H., Komppula, M., Laj, P., Li, S. M., Lunder, C., Marinoni, A., Martins Dos Santos, S., Moerman, M., Nowak, A., Ogren, J. A., Petzold, A., Pichon, J. M., Rodriquez, S., Sharma, S., Sheridan, P. J., Teinilä, K., Tuch, T., Viana, M., Virkkula, A., Weingartner, E., Wilhelm, R. and Wang, Y. Q.: Characterization and intercomparison of aerosol absorption photometers: Result of two intercomparison workshops, Atmos. Meas. Tech., 4(2), 245–268, doi:10.5194/amt-4-245-2011, 2011.

Myhre, G., Samset, B.H., Schulz, M., Balkanski, Y., Bauer, S., Berntsen, T.K., Bian, H., Bellouin, N., Chin, M., Diehl, T., Easter, R.C., Feichter, J., Ghan, S.J., Hauglustaine, D., Iversen, T., Kinne, S., Kirkeväg, A., Lamarque, J.F., Lin, G., Liu, X., Lund, M.T., Luo, G., Ma, X., Van Noije, T., Penner, J.E., Rasch, P.J., Ruiz, A., Seland, Skeie, R.B., Stier, P., Takemura, T., Tsigaridis, K., Wang, P., Wang, Z., Xu, L., Yu, H., Yu, F., Yoon, J.H., Zhang, K., Zhang, H. and., Zhou, C.:., 2013. Radiative forcing of the direct aerosol effect from AeroCom Phase II simulations,. Atmos. Chem. Phys.,. 13(4),. 1853–1877, . https://doi:.org/10.5194/acp-13-1853-2013, 2013.

Ogren, J. A.: Comment on "Calibration and Intercomparison of Filter-Based Measurements of Visible Light Absorption by Aerosols," Aerosol Sci. Technol., 44(8), 589–591, doi:10.1080/02786826.2010.482111, 2010.

Petrakakis, M. J., Kelessis, A. G., Tzoumaka, P., and Samara, C.: Levels of Suspended Particulate Matter before and after the Economic Crisis in Thessaloniki, Greece, Proceedings of 17th International Symposium on Environmental Pollution and its Impact on Life in the Mediterranean Region, Istanbul, Turkey, 28September–1 October, Mediterranean Scientific Association of Environmental Protection (MESAEP), 2013.

Petzold, A. and Petzold, A., Schönlinner, M.:., 2004. Multi-angle absorption photometry - A new method for the measurement of aerosol light absorption and atmospheric black carbon,. J. Aerosol Sci.,. 35(4),. 421–441, .

https://doi:.org/10.1016/j.jaerosci.2003.09.005, 2004.
Petzold, A., Onasch, T., Kebabian, P. and Freedman, A.: Intercomparison of a Cavity Attenuated Phase Shift-based extinction monitor (CAPS PMex) with an integrating nephelometer and a filter-based absorption monitor, Atmos. Meas. Tech., 6(5), 1141–1151, doi:10.5194/amt-6-1141-2013, 2013.
Pikridas, M., Tasoglou, A., Florou, K. and, Pandis, S.N.:, 2013. Characterization of the origin of fine particulate matter in a medium size urban area in the Mediterranean, Atmos. Environ., 80, 264–274, https://doi:.org/10.1016/j.atmosenv.2013.07.070, 2013.
Pikridas, M., Vrekoussis, M., Sciare, J., Kleanthous, S., Vasiliadou, E., Kizas, C., Savvides, C. and, Mihalopoulos, N.:, 2018. Spatial and temporal (short and long-term) variability of submicron, fine and sub-10 μm particulate matter (PM1, PM2.5, PM10) in Cyprus, Atmos. Environ., 191, 79–93, https://doi:.org/https://doi.org/10.1016/j.atmosenv.2018.07.048, 2018.
Ramachandran, S. and Rajesh, T. A.: Black carbon aerosol mass concentrations over Ahmedabab, an urban location in western India: Comparison with urban sites in Asia, Europe, Canada, and the United States, J. Geophys. Res. Atmos., 112(6), 1–19, doi:10.1029/2006JD007488, 2007.
Ran, L., Deng, Z., Xu, X., Yan, P., Lin, W., Wang, Y., Tian, P., Wang, P., Pan, W. and Lu, D.: Vertical profiles of black carbon measured by a micro-aethalometer in summer in the North China Plain, Atmos. Chem. Phys., 16(16), 10441–10454, doi:10.5194/acp-16-10441-2016, 2016.
Saffari, A., Daher, N., Samara, C., Voutsa, D., Kouras, A., Manoli, E., Karagkiozidou, O., Vlachokostas, C., Moussiopoulos, N., Shafer, M. M., Schauer, J. J. and Sioutas, C.: Increased biomass burning due to the economic crisis in Greece and its adverse impact on wintertime air quality in Thessaloniki, Environ. Sci. Technol., 47(23), 13313–13320, doi:10.1021/es403847h, 2013.
Samset, B. H., Stjern, C. W., Andrews, E., Kahn, R. A., Myhre, G., Schulz, M. and Schuster, G. L.: Aerosol Absorption: Progress Towards Global and Regional Constraints, Curr. Clim. Chang. Reports, 4(2), 65–83, doi:10.1007/s40641-018-0091-4, 2018.
Sandradewi, J., Prévôt, A.S.H., Szidat, S., Perron, N., Alfarra, M.R., Lanz, V.A., Weingartner, E. and, Baltensperger, U.R.S.:, 2008. Using aerosol light abosrption measurements for the quantitative determination of wood burning and traffic emission contribution to particulate matter, Environ. Sci. Technol., 42(9), 3316–3323, . https://doi:.org/10.1021/es702253m, 2008.
Schrod, J., Weber, D., Drücke, J., Keleshis, C., Pikridas, M., Ebert, M., Cvetković, B., Nickovic, S., Marinou, E., Baars, H., Ansmann, A., Vrekoussis, M., Mihalopoulos, N., Sciare, J., Curtius, J. and, Bingemer, H.G.:, 2017. Ice nucleating particles over the Eastern Mediterranean measured by unmanned aircraft systems, Atmos. Chem. Phys., 17(7), 4817–4835, . https://doi:.org/10.5194/acp-17-4817-2017, 2017.
Sedlacek, A.J., Buseck, P.R., Adachi, K., Onasch, T.B., Springston, S.R. and, Kleinman, L.:, 2018. Formation and evolution of tar balls from northwestern US wildfires, Atmos. Chem. Phys., 18(15), 11289–11301, https://doi:.org/10.5194/acp-18-11289-2018, 2018.
Seinfeld, J. H., Carmichael, G. R., Arimoto, R., Conant, W. C., Brechtel, F. J., Bates, T. S., Cahill, T. A., Clarke, A. D., Doherty, S. J., Flatau, P. J., Huebert, B. J., Kim, J., Markowicz, K. M., Quinn, P. K., Russell, L. M., Russell, P. B., Shimizu, A., Shinozuka, Y., Song, C. H., Tang, Y., Uno, I., Vogelmann, A. M., Weber, R. J., Woo, J. H. and Zhang, X. Y.: ACE-ASIA: Regional climatic and atmospheric

chemical effects of Asian dust and pollution, Bull. Am. Meteorol. Soc., 85(3), 367–380, doi:10.1175/BAMS-85-3-367, 2004.

Sheridan, P.J., Patrick Arnott, W., Ogren, J.A., Andrews, E., Atkinson, D.B., Covert, D.S., Moosmüller, H., Petzold, A., Schmid, B., Strawa, A.W., Varma, R. and., Virkkula, A.:, 2005. The reno aerosol optics study: An evaluation of aerosol absorption measurement methods,. Aerosol Sci. Technol.,. 39(1),. 1–16, . https://doi:.org/10.1080/027868290901891, 2005.

Shiraiwa, M., Kondo, Y., Iwamoto, T. and Kita, K.: Amplification of light absorption of black carbon by organic coating, Aerosol Sci. Technol., 44(1),. 46–54, doi:DOI: 10.1080/02786820903357686, 2010.

Slowik, J. G., Cross, E. S., Han, J. -H., Davidovits Davidotis, P., Onasch, T. B., Jayne, J. T., Williams, L. R., Canagaratna, M. R., Worsnop, D. R., Chakrabarty, R. K., Moosmüller, H., Arnott, W. P., Schwarz, J. P., Gao, R. S. K., Fahey, D. W., Kok, G. L. and., Petzold, A.: An Inter-Comparison intercomparison of Instruments Measuring Black Carbon Content instruments measuring black carbon content of Soot Particles soot particles, Aerosol Sci. Technol., 41(3),. 295–314, doi:DOI: 10.1080/02786820701197078, 2007.

Subramanian, R., Kok, G. L., Baumgardner, D., Clarke, A., Shinozuka, Y., Campos, T. L., Heizer, C. G., Stephens, B. B., De Foy, B., Voss, P. B. and Zaveri, R. A.: Black carbon over Mexico: The effect of atmospheric transport on mixing state, mass absorption cross-section, and BC/CO ratios, Atmos. Chem. Phys., 10(1), 219–237, doi:10.5194/acp-10-219-2010, 2010.

US Department of Transportation, Federal Aviation Administration, "CFR-code of federal regulations title 14", Registration and Marking Requirements for Small Unmanned Aircraft Part 48, 2015. Available at https://www.faa.gov/news/updates/media/20151213_IFR.pdf (last access 25 September 2019)

Villa, T. F., Gonzalez, F., Miljievic, B., Ristovski, Z. D. and Morawska, L.: An overview of small unmanned aerial vehicles for air quality measurements: Present present applications and future prospectives, Sensors (Switzerland),. 16(7),. 1072, doi:10.3390/s16071072, 2016.

Virkkula, A., Ahlquist, N.C., Covert, D.S., Arnott, W.P., Sheridan, P.J., Quinn, P.K. and., Coffman, D.J.: Modification, calibration and a field test of an instrument for measuring light absorption by particles,. Aerosol Sci. Technol.,. 39(1),. 68–83, doi:10.1080/027868290901963, 2005.

Virkkula, A., Chi, X., Ding, A., Shen, Y., Nie, W., Qi, X., Zheng, L., Huang, X., Xie, Y., Wang, J., Petäjä, T. and Kulmala, M.: On the interpretation of the loading correction of the aethalometer, *Atmos. Meas. Tech.*,8, 4415-4427, doi:10.5194/amt-8-4415-2015, 2015.

Wang, R., Balkanski, Y., Boucher, O., Ciais, P., Schuster, G. L., Chevallier, F., Samset, B. H., Liu, J., Piao, S., Valari, M. and., Tao, S.: Estimation of global black carbon direct radiative forcing and its uncertainty constrained by observations, J. Geophys. Res. *Atmos.*, 121(10),. 5948–5971, doi:10.1002/2015JD024326,:10.1002/2015JD024326, 2016.

Watson, J. G., Chow, J. C.,. and Chen, L.-W. A.: Summary of Organic organic and Elemental Carbon/Black Carbon Analysis Methods elemental carbon/black carbon analysis methods and Intercomparisons.,intercomparisons, *Aerosol Air Qual. Res.*, 5, 65–102, 2005.

Weingartner, E., Saathoff, H., Schnaiter, M., Streit, N., Bitnar, B. and Baltensperger, U.: Absorption of light by soot particles: Determination determination of the

absorption coefficient by means of aethalometers, J. Aerosol Sci., 34(10),, 1445–1463, doi:10.1016/S0021-8502(03)00359-8, 2003.

Welch, B. L.: The generalization of 'Student's' problem when several different population variances are involved, Biometrika, 34(1–2), 28–35, doi:10.1093/biomet/34.1-2.28, 1947.

Wilcox, E.M., Thomas, R.M., Praveen, P.S., Pistone, K., Bender, F.A.-M. and, Ramanathan, V.:, 2016. Black carbon solar absorption suppresses turbulence in the atmospheric boundary layer, Proc. Natl. Acad. Sci., 113(42), 11794–11799, https://doi.org/10.1073/pnas.1525746113, 2016.

Zhang, H., Zhou, C., Wang, Z., Zhao, S. and Li, J., Jiangnan, L.: The influence of different black carbon and sulfate mixing methods on their optical and radiative properties, J. Quant. Spectrosc. Radiat. Transf., *Transfer,* 161, 105–116, http://dx.doi.org/10.1016/j.jqsrt.2015.04.002, 2015.

Zhang, Y., Favez, O., Canonaco, F., Liu, D., Močnik, G., Amodeo, T., Sciare, J., Prévôt, A. S. H., Gros, V. and Albinet, A.: Evidence of major secondary organic aerosol contribution to lensing effect black carbon absorption enhancement, npj Clim. Atmos. Sci., 1(1), doi:10.1038/s41612-018-0056-2, 2018.

Zíková, N., Vodička, P., Ludwig, W., Hitzenberger, R., Schwarz, J., 2016. On the use of the field Sunset semi-continuous analyzer to measure equivalent black carbon concentrations. Aerosol Sci. Technol. 50, 284–296. https://doi.org/10.1080/02786826.2016.1146819

Table 1. Summary of UAS used during the Athens and Cyprus campaigns. A UAS is considered small if its gross weight is smaller than 25 kg and medium if its gross weight ranges between 25 and 50 kg.

USRL Fleet of UAS	Type	MTOW†	Payload*	Endurance*	Ceiling*	Manufacturer
 Cruiser	Medium Size Fixed Wing	35 kg	12 kg	4 h	3km a.s.l. ~~3k asl~~	ET-Air
 Skywalker X8	Small Size Fixed Wing	5 kg	3 kg	1 h	3 km a.s.l.~~asl~~	Skywalker
 DJi S1000+	Small Size Rotary Wing	11 kg	4 kg	30 min	1 km a.s.l.~~asl~~	DJi

* UAS characteristics as configured particularly for these studies (BACCHUS and ACTRIS campaigns).
† Maximum take-off weight

Table 2. Summary of standardized properties of each attenuation monitor. The term λ refers to the wavelength used in nm.

~~Manufacturer~~Instrument name	~~Instrument name~~Manufacturer	Mass attenuation cross section (m^2 g^{-1})	Optical enhancement factor (C)	Reference
~~Magee Scientific~~AE33	~~AE33~~Magee Scientific	10730.48/λ	1.57	Drinovec et al., 2015
~~Magee Scientific~~AE51	~~AE51~~Magee Scientific	11000/λ	2.05	Ferrero et al., 2011
STAP~~Brechtel~~	Brechtel~~STAP~~	N/A*	N/A*	Ogren et al., 2010
~~Thermo Scientific~~MAAP	~~MAAP~~Thermo Scientific	6.6 at 670 nm	N/A	Petzold and Schönlinner, 2004
~~Custom made from AE51~~Dual Wavelength Prototype (DWP)	~~Dual Wavelength Prototype (DWP)~~Custom made from AE51	11000/λ	2.05	N/A

* Equation 7 is used instead

Table 3. Characteristics of the miniature absorption instruments.

Instrument Name	Flowrate (LPM)	Spot Area (m^2)	Wavelengths (nm)	Face Velocity ($m\ s^{-1}$)	Weight* (g)	Time Response (s)
AE51	0.1-0.2	7.1×10^{-6}	880	0.5	280	1, 10, 30
DWP	2	7.1×10^{-6}	370, 880	4.7	1100	1
STAP	1.3	17.7×10^{-6}	445, 515,633	1.2	660	1

*Refers to the weight of the instrument alone. Dryer and sampling inlet used are not accounted for.

Table 4. Results from the comparison of the miniature sensors with ground -based commercial instruments (AE33 and MAAP) shown in Fig. 5~~, 6~~ and 6~~7~~

	eBC		$b_{abs}(370)$ *Mm*$^{-1}$		$b_{abs}(880)$ *Mm*$^{-1}$		*Ångström~~Angstrom~~ Exponent*	
	slope ±95% CI	**Quality of fit (R^2)**	**slope ±95% CI**	**Quality of fit (R^2)**	**slope ±95% CI**	**Quality of fit (R^2)**	**slope ±95% CI**	**Quality of fit (R^2)**
				Athens campaign				
AE33	1.20±0.11	0.98	2.45±0.21	0.99	2.25±0.19	0.99	N/A	N/A
DWP	0.93±0.15	0.90	1.22±0.20	0.87	1.29±0.20	0.90	0.87±0.22	0.21
AE51	0.94±0.09	0.76	N/A	N/A	1.30±0.12	0.76	N/A	N/A
STAP	N/A	N/A	0.93±0.07	0.89	1.06±0.08	0.88	0.88±0.17	0.27
				Cyprus campaign				
AE33	1.13±0.05	0.89	1.93±0.09	0.88	1.83±0.08	0.89	N/A	N/A
DWP	0.94±0.20	0.71	0.83±0.18	0.68	1.20±0.26	0.71	0.44±0.28	0.1
AE51	1.22±0.52	0.32	N/A	N/A	1.55±0.66	0.32	N/A	N/A


100m
12m

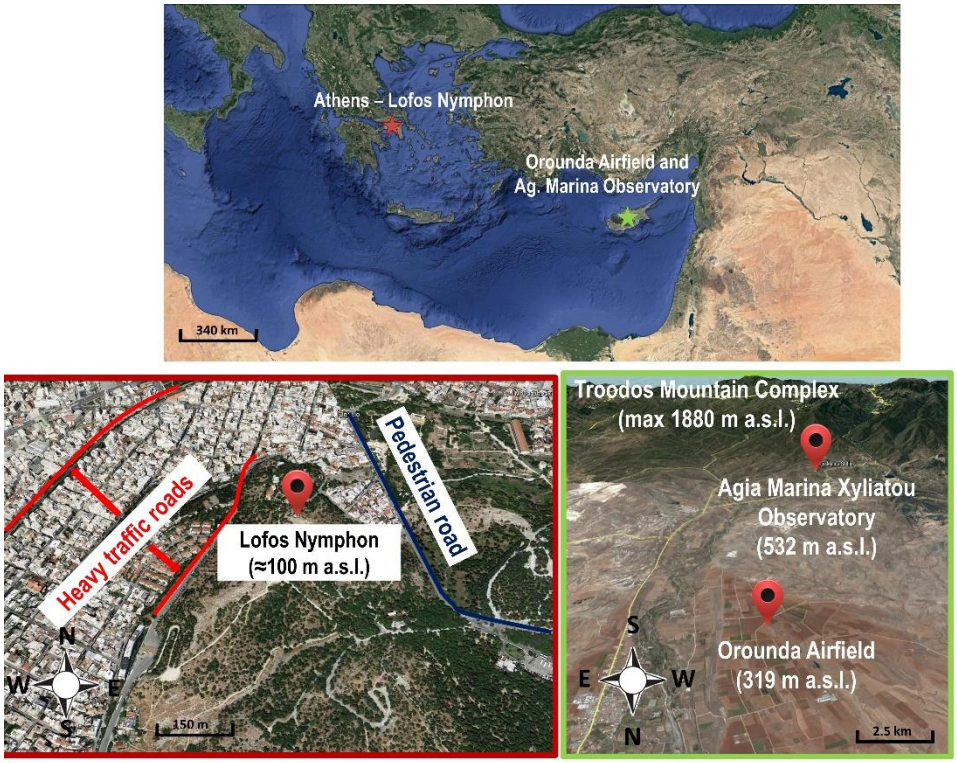

Figure 1: Aerial view of the Orounda runway in Cyprus.

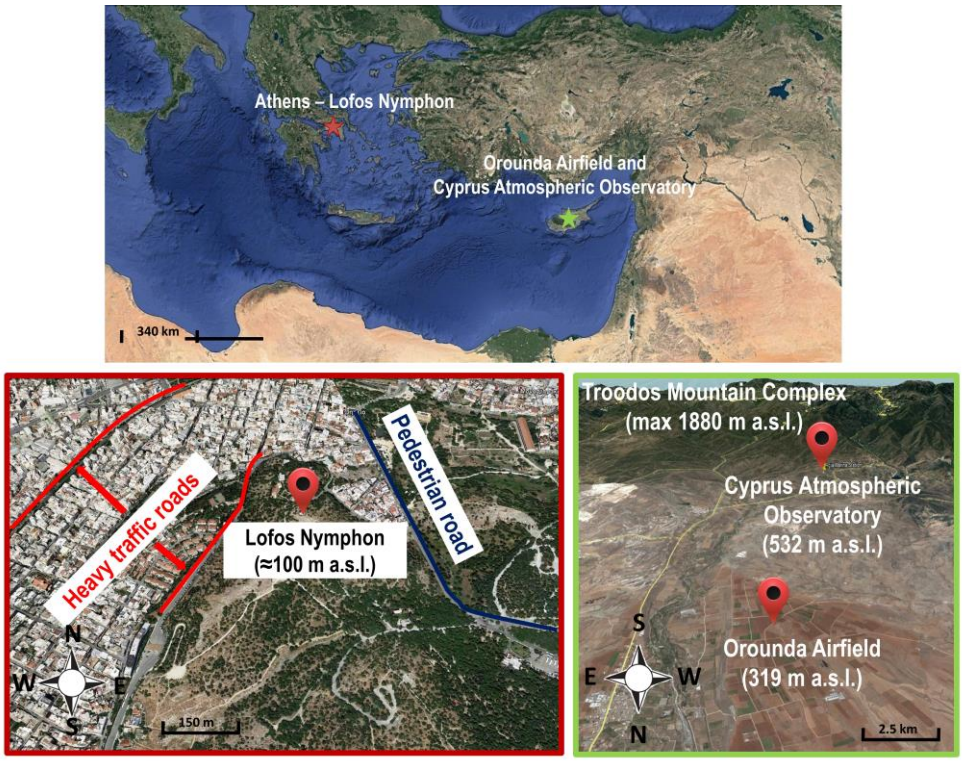

Figure 2. Upper panel: Location of the two sampling sites in the Eastern Mediterranean (top).) ~~of the two sampling sites.~~ During the Athens campaign, sampling was conducted at Lofos Nymphon (bottom left) surrounded by busy traffic roads (red line) and a touristic area (blue line) free of motor vehicles. During the Cyprus campaign, (bottom right) measurements using UAS was conducted at the Orounda airfield and ground -based monitoring at the Cyprus atmospheric observatory (close to Agia Marina Xyliatou)~~Xyliatoy Observatory~~ at the foothills of the Troodos mountains.~~mountain complex.~~ The elevation difference between these sites is noted. All images are courtesy of Google Maps.

Figure 2: Aerial view of the Orounda runway in Cyprus.

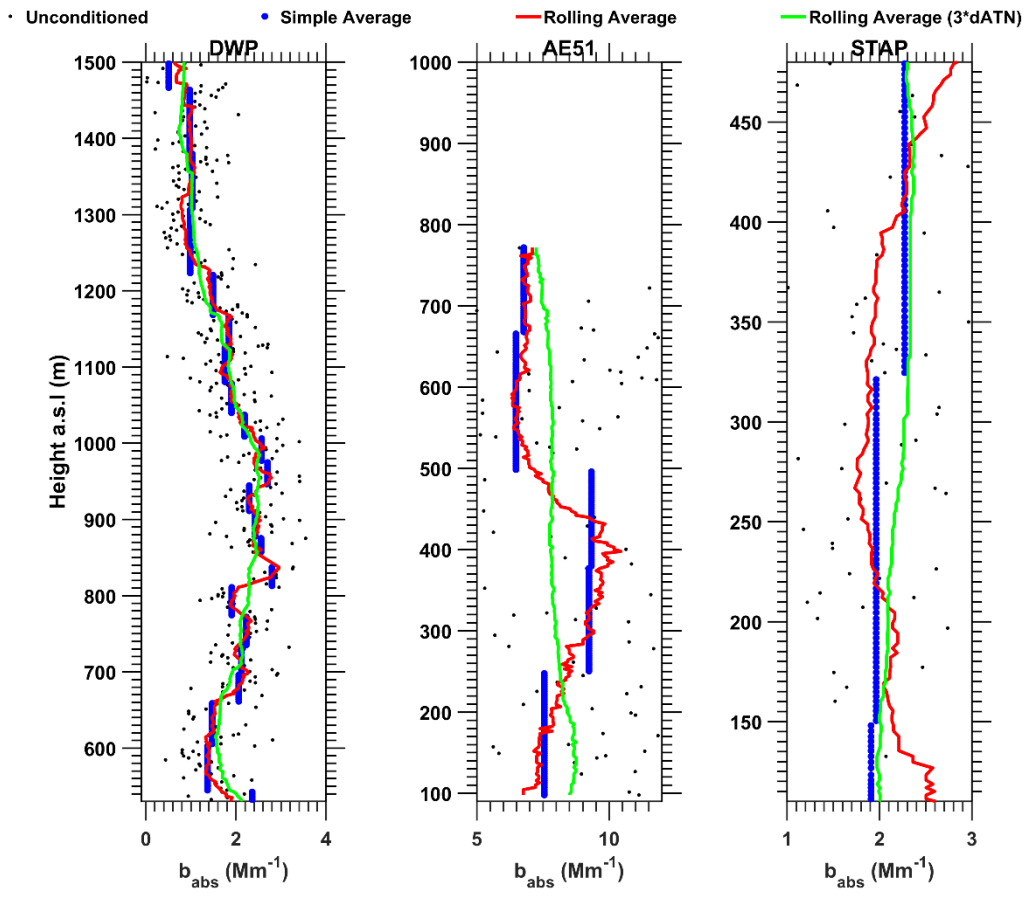

Figure 3. Examples of the use of the improved ONA algorithm for the three attenuation monitors examined in this study. Raw data (black dots) are shown against the traditional ONA algorithm (Hagler et al., 2011; blue ~~dots~~), the improved ONA using a rolling average and the ΔATN proposed in Section 4~~5~~ (red ~~line~~), and the improved ONA using the rolling average but with increased ΔATN by a factor of 3 (over-smoothed~~oversmoothed~~ green ~~line~~). The proposed ΔATN used are 0.01, 0.03, 0.03 for AE51, DWP and STAP, respectively.

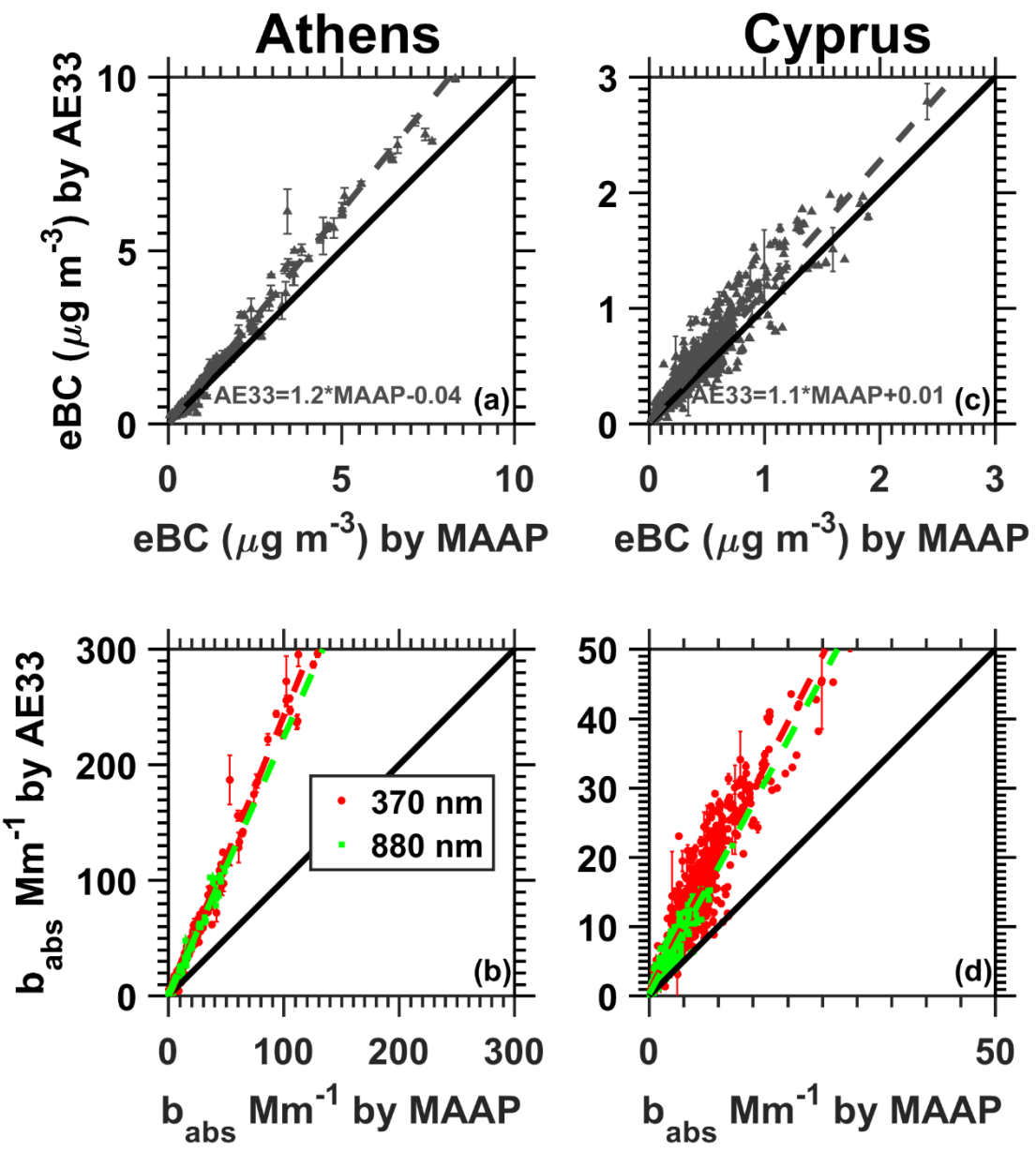
Athens
Cyprus
eBC (μg m-3) by AE33
eBC (μg m-3) by MAAP
AE33=1.2*MAAP-0.04
(a)
AE33=1.1*MAAP+0.01
(c)
babs Mm-1 by AE33
babs Mm-1 by MAAP
370 nm
880 nm
(b)
(d)

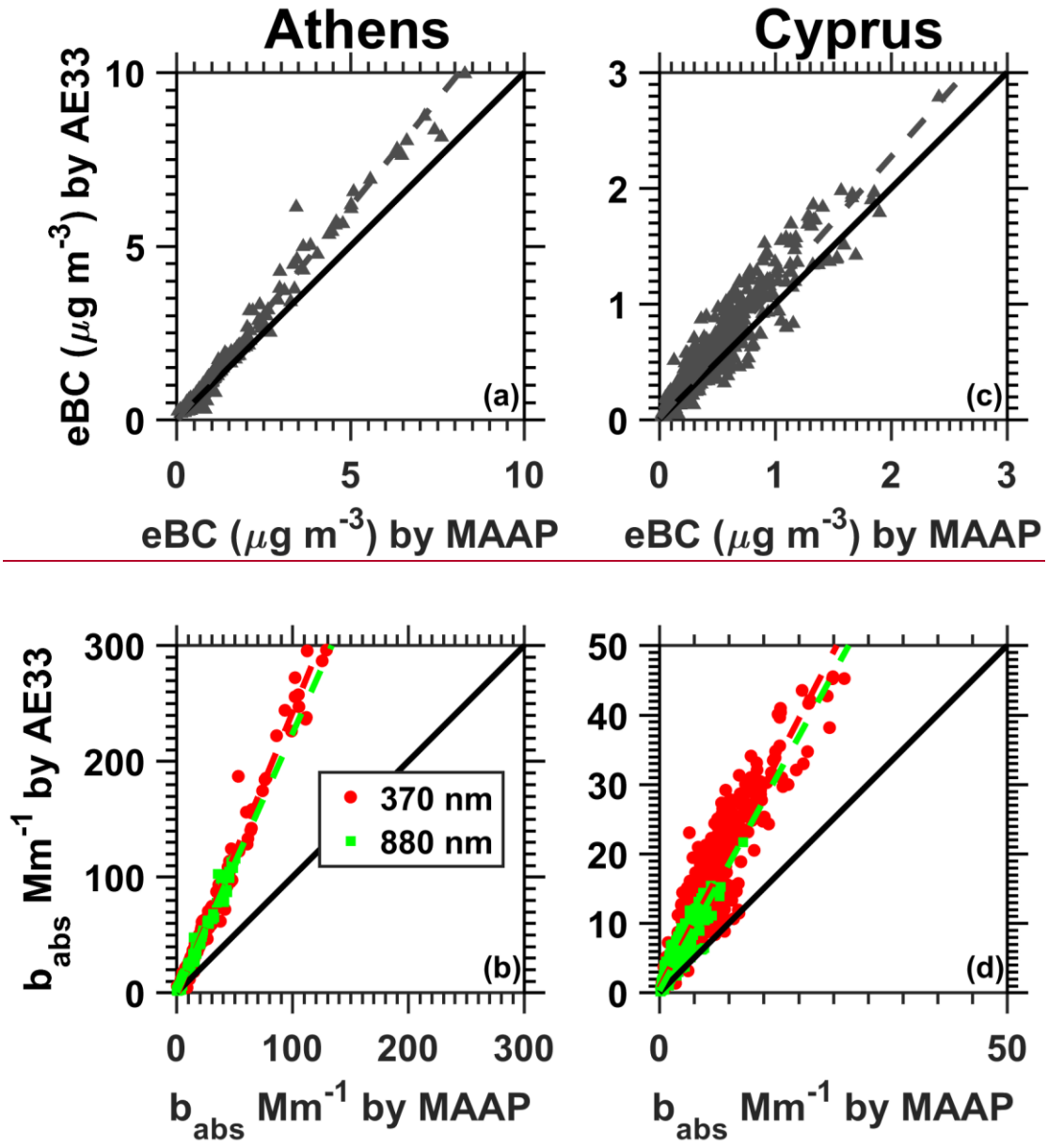

Figure 4. Comparison of AE33 against MAAP for eBC (a,c panels) and b_{abs} (b, d panels) at 370nm (red dots) and 880nm (green dots) during the Athens (a, b~~c~~ panels) and Cyprus (c, ~~b,~~d panels) campaigns, respectively. Error bars correspond to one standard error from the mean. Not visible error bars suggest that the error estimate is smaller than the area covered by the symbol. The 1:1 and regression lines are shown by a solid black and a dashed line colored accordingly to the instrument, respectively. Results are shown in Table 4.

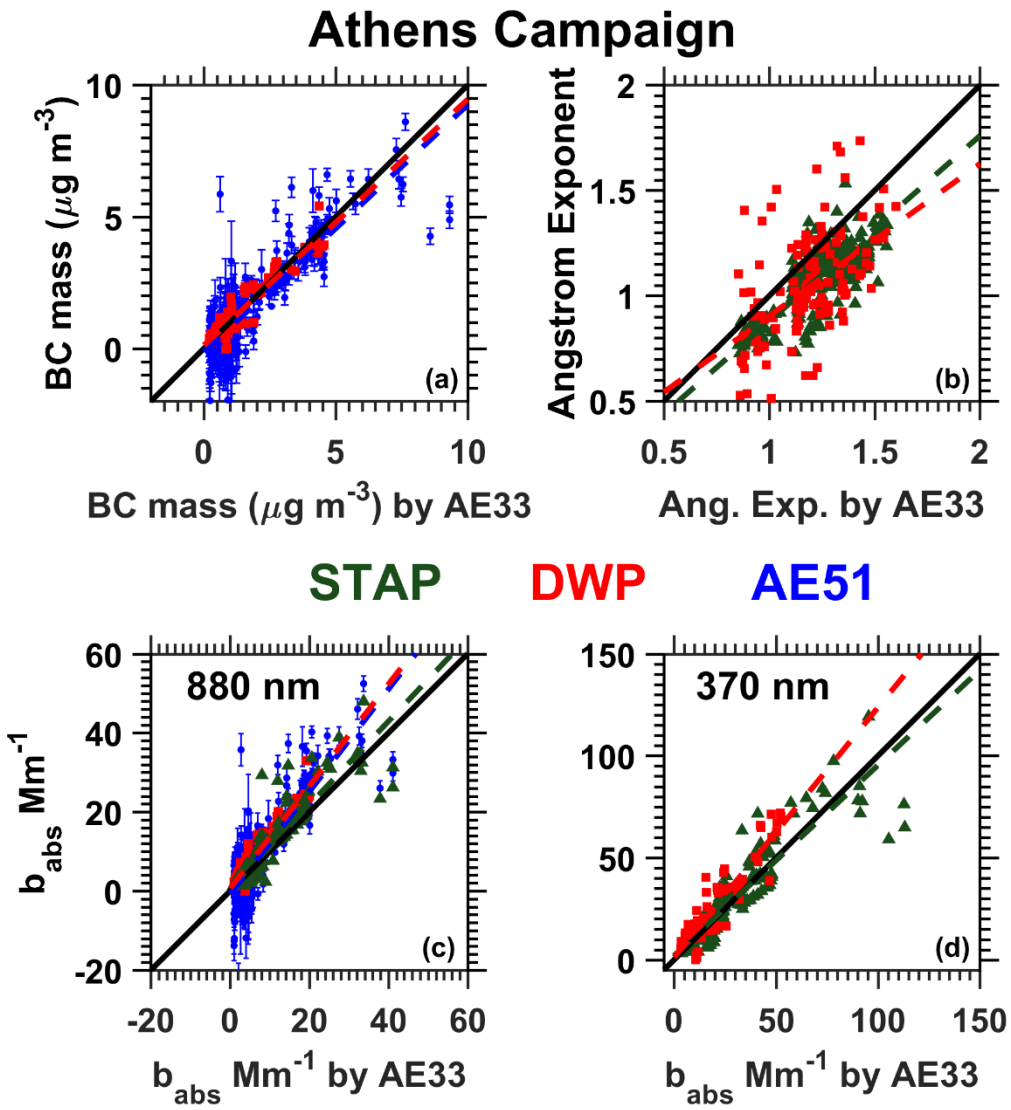
Athens Campaign
BC mass (μg m-3)
BC mass (μg m-3) by AE33
(a)
Angstrom Exponent
Ang. Exp. by AE33
(b)
STAP
DWP
AE51
880 nm
babs Mm-1
babs Mm-1 by AE33
(c)
370 nm
babs Mm-1 by AE33
(d)

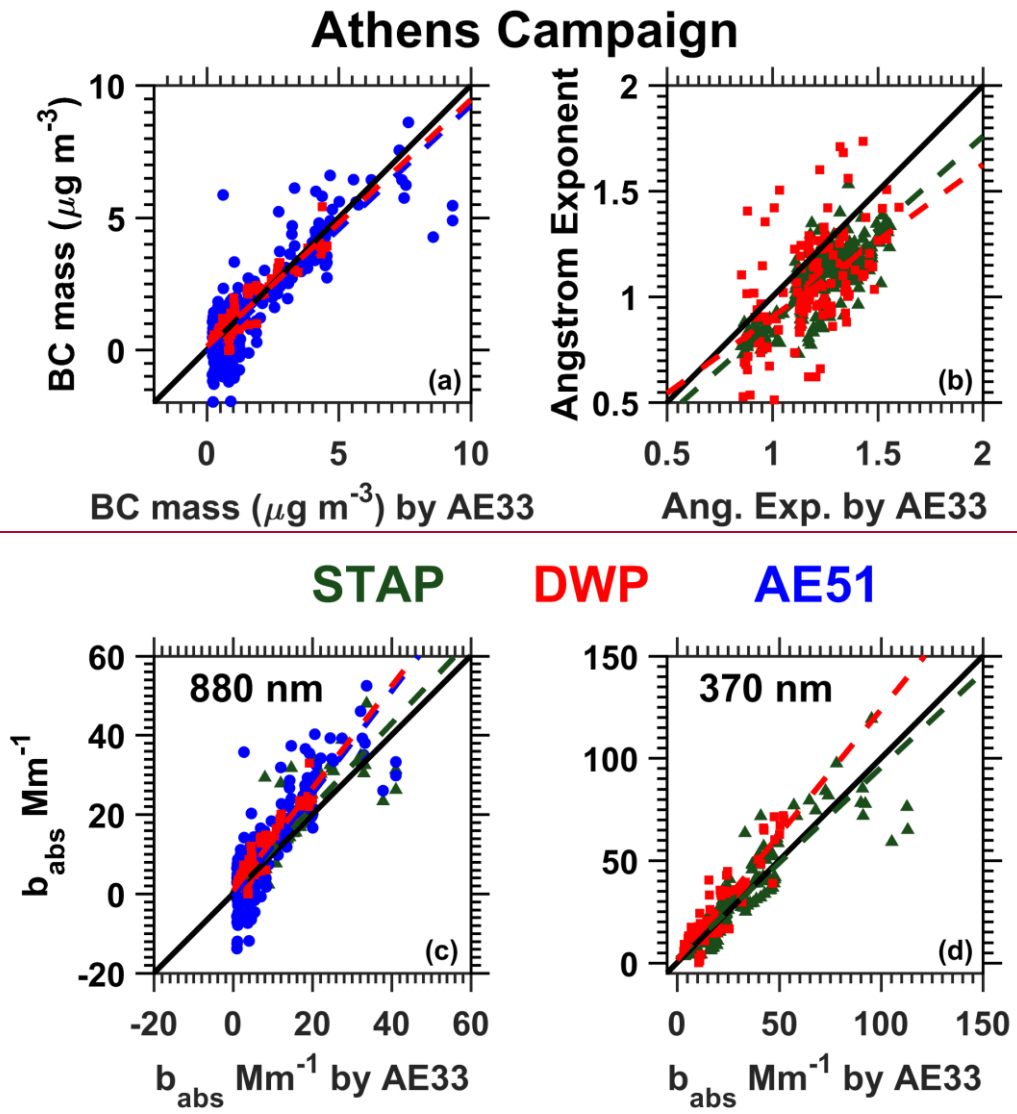

Figure 5. Comparison of miniature ~~attenuation~~ monitors (STAP: green triangles; DWP: red squares; AE51: blue circles) whilst on the ground against the corrected AE33 during the Athens campaign with respect to *eBC* mass (a), absorption Ångström~~angstrom~~ exponent (b), ~~and~~ the absorption coefficient at 880 nm (c) and 370 nm (d). Error bars correspond to one standard error from the mean with respect to AE51. The standard error concerning DWP and STAP with respect b_{abs} and *eBC* is smaller than the symbol in the graph for the vast majority of the cases and is not presented for clarity. The 1:1 and regression lines are shown by a solid black and a dashed line colored accordingly to the instrument, respectively. Results are shown in Table 4.

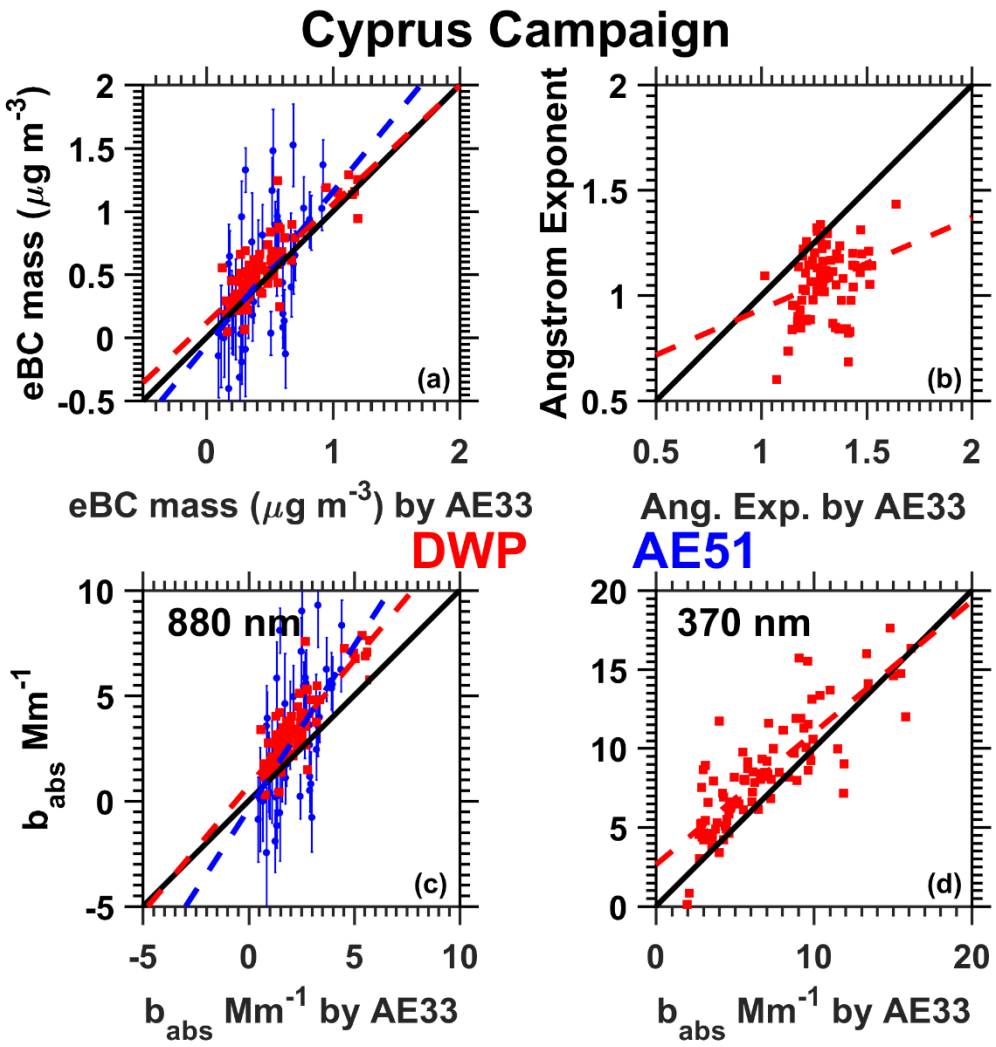
Cyprus Campaign
eBC mass (μg m-3)
(a)
eBC mass (μg m-3) by AE33
Angstrom Exponent
(b)
Ang. Exp. by AE33
DWP
AE51
880 nm
babs Mm-1
(c)
babs Mm-1 by AE33
370 nm
(d)
babs Mm-1 by AE33

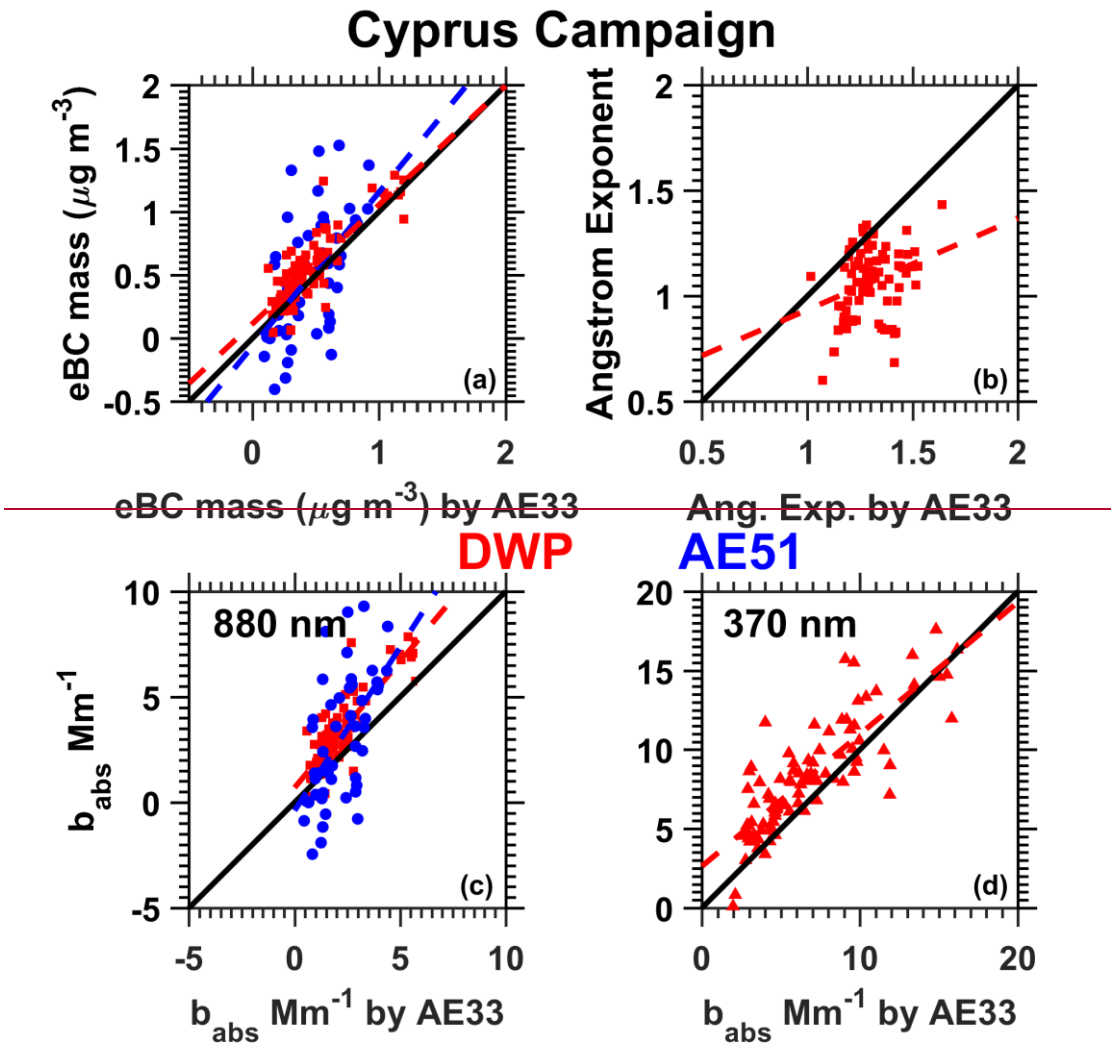

Figure 6. Comparison of miniature attenuation monitors (DWP: red squares; AE51: blue circles) while airborne against the corrected AE33 during the Cyprus campaign with respect to eBC mass (a), absorption Ångström~~angstrom~~ exponent (b), and the absorption coefficient at 880 nm (c) and 370 nm (d). Miniature monitors sampled airborne. Error bars correspond to one standard error from the mean with respect to AE51. The standard error concerning DWP and STAP with respect b_{abs} and *eBC* is smaller than the symbol in the graph for the vast majority of the cases and is not presented for clarity. The 1:1 and regression lines are shown by a solid black and a dashed line colored accordingly to the instrument, respectively. Results are shown in Table 4. ~~Results are shown in Table 4.~~

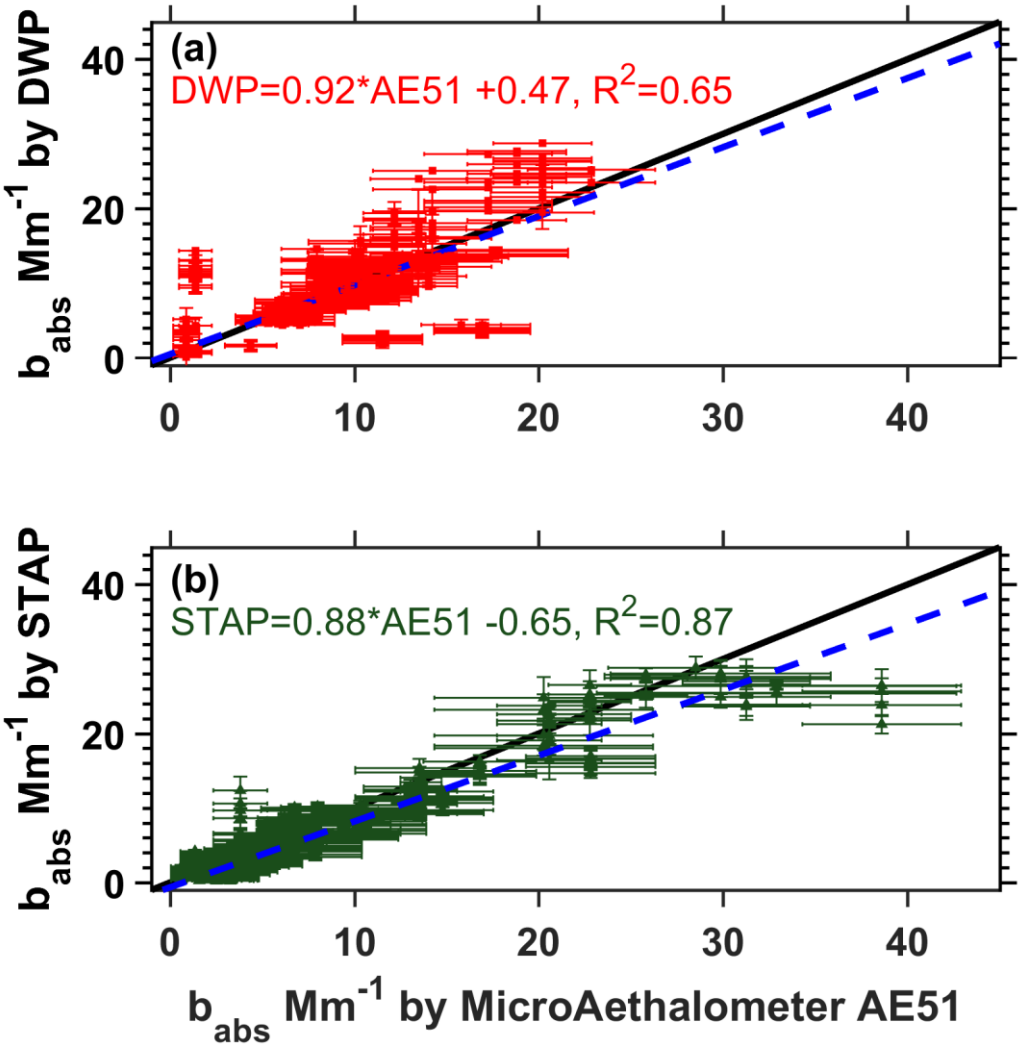
(a)
DWP=0.92*AE51 +0.47, R2=0.65
babs Mm-1 by DWP
(b)
STAP=0.88*AE51 -0.65, R2=0.87
babs Mm-1 by STAP
babs Mm-1 by MicroAethalometer AE51
0
10
20
30
40

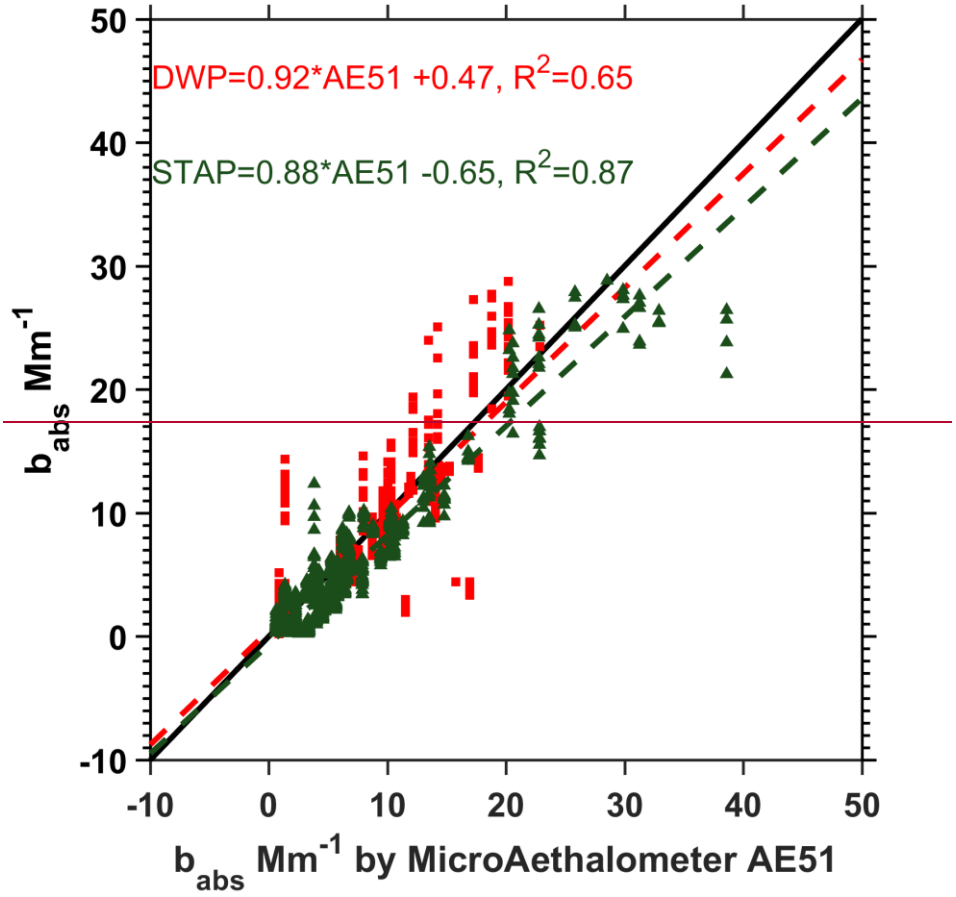

Figure 7. Comparison of AE51 against STAP (green triangles) and DWP (red~~magenta~~ squares) during eight flights of the Athens campaign. The reported agreement in the correlation suggests that no significant bias affected the monitors. The correlation deteriorates ~~to~~ (R^2=0.01) if data are not processed with the noise reduction algorithm (~~conditioned as suggested in~~ Section 4). Error bars correspond to one standard error from the mean. Not visible error bars suggest that the smoothing algorithm did not average that sampling point with its neighbors, resulting in a standard deviation and standard error equal to zero. The 1:1 and regression lines are shown by a solid black and a dashed blue line, respectively.~~5.~~

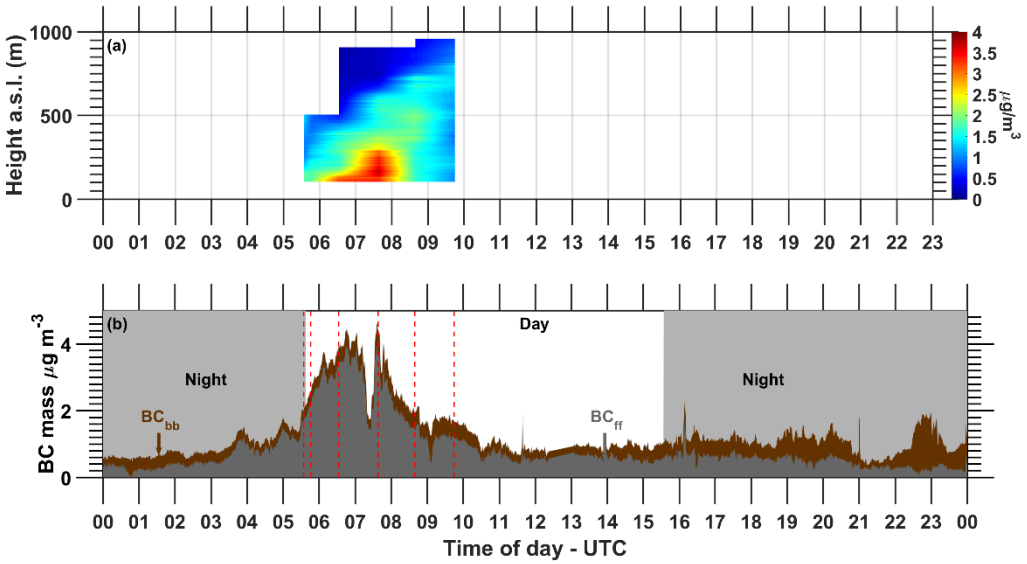

Figure 8. Reconstruction of *eBC* mass vertical distribution (a) based on 6 flights between 19th January 2016 (Athens campaign) 05:30 and 09:30 (UTC). The lidar-determined~~actual~~ vertical distributions are shown in Fig. 9. The corresponding ground measurements are also shown on panel (b). The concentration of BC from fossil fuel (ff) and biomass burning (bb) are shown with grey and brown color~~colour~~, respectively. Dashed red lines indicate the start of each of the 6 flights the reconstructed *eBC* profiles was based upon.

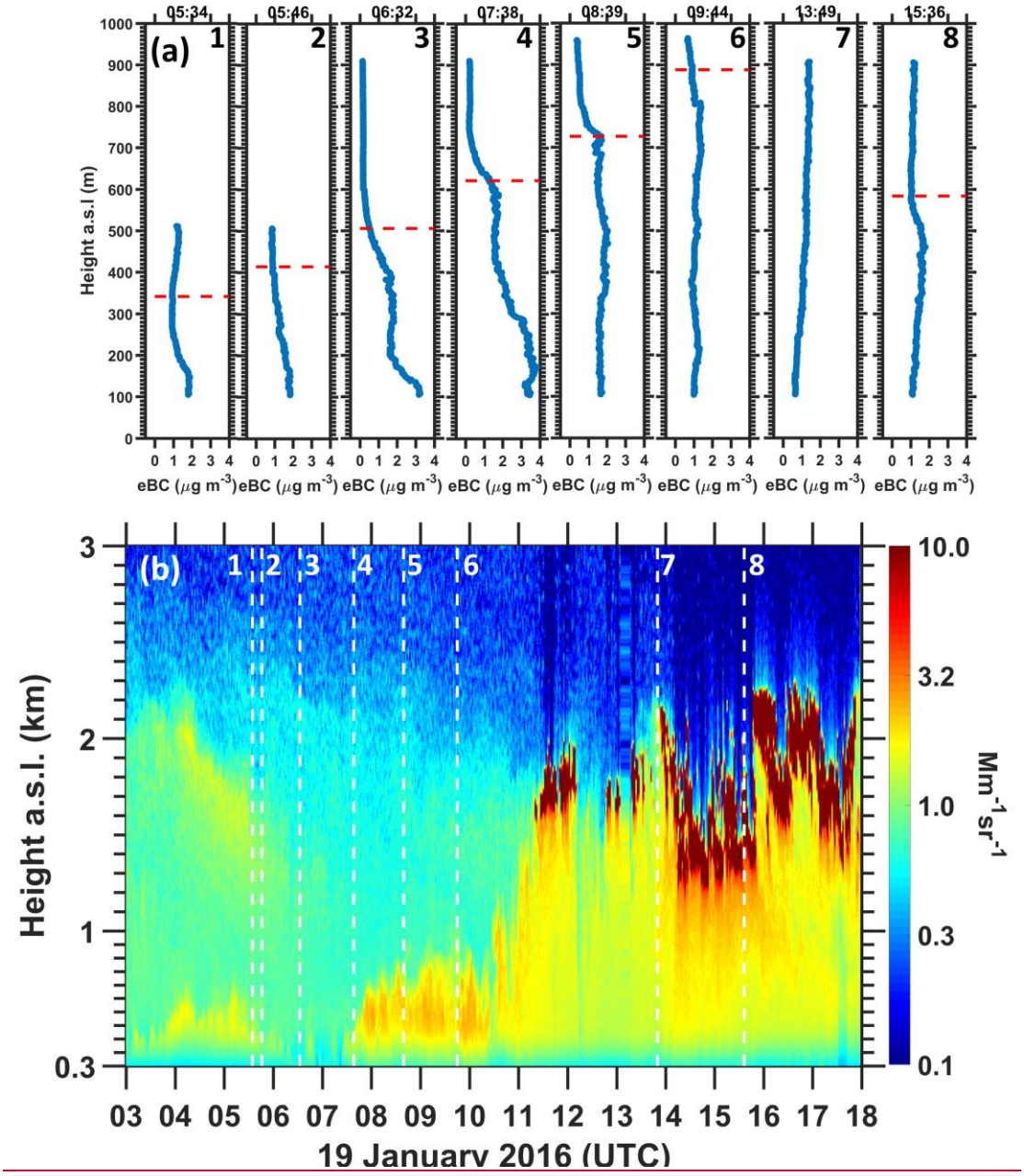
(a)
05:34
05:46
06:32
07:38
08:39
09:44
13:49
15:36
1
2
3
4
5
6
7
8
Height a.s.l (m)
eBC (μg m-3)
(b)
Height a.s.l. (km)
10.0
3.2
1.0
0.3
0.1
Mm-1 sr-1
19 January 2016 (UTC)

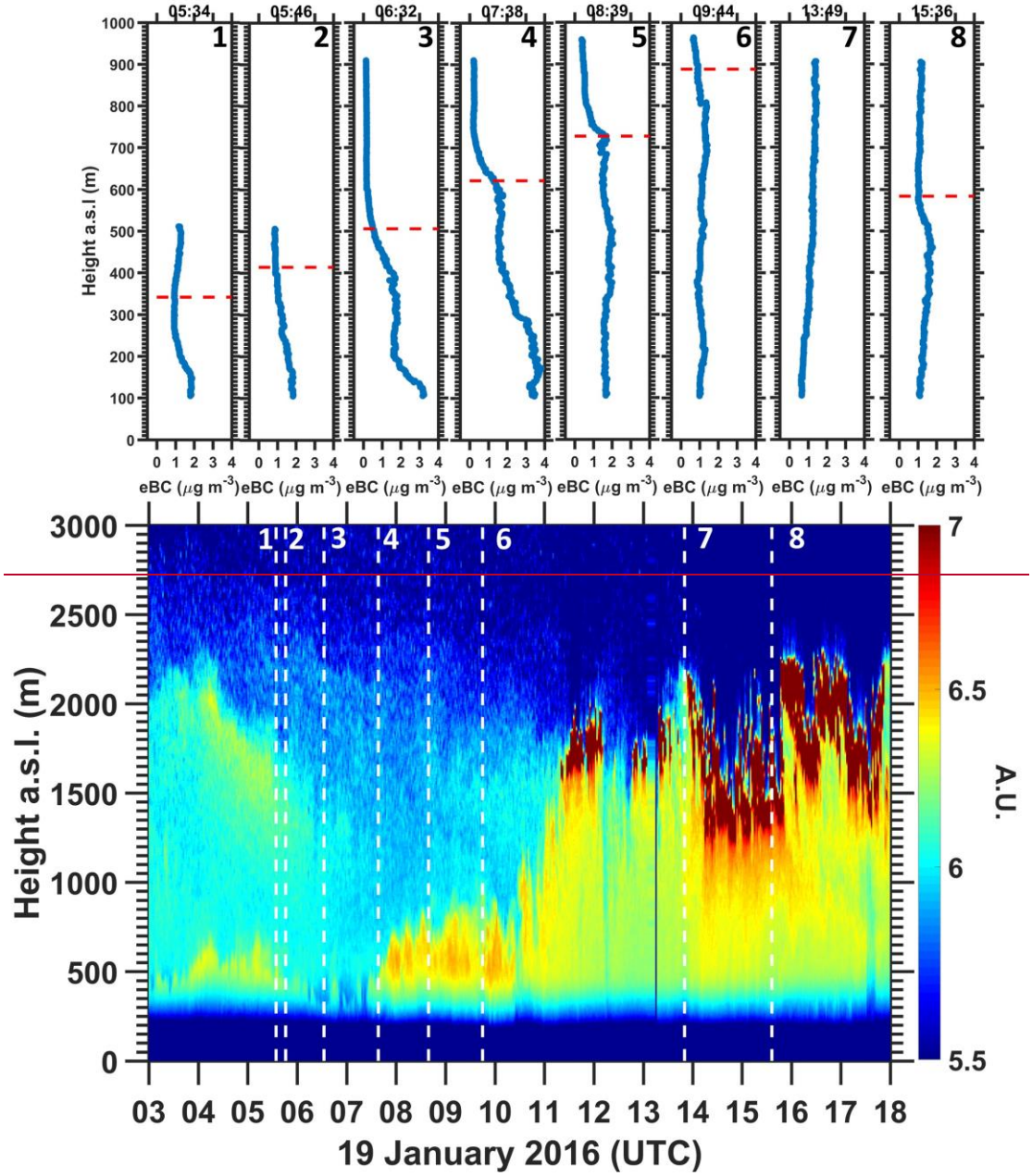

Figure 9. Vertical profiles (blue lines) of the *eBC* mass (a),~~.~~ measured during 19th January 2016 (Athens campaign) accompanied by the mixing height (dashed red line) of the lower layer derived by Polly-XT measurements. During the 13:49 flight, mixing height was higher than the maximum altitude of flight and it is not shown. The corresponding time-height display of the 1064-nm attenuated backscatter~~range corrected signal~~ measured with Polly-XT is also shown (b).~~.~~ Dashed white lines correspond to the start of each of the 8 flights performed during that day.